Carbon and nitrogen fluxes in the marine coccolithophore *Emiliania huxleyi* grown under different nitrate concentrations

by

Athanasios Kaffes

A thesis submitted in partial fulfillment

of the requirements for the degree of

Doctor of Philosophy

in Marine Biology

Approved, Thesis committee

Prof. Dr. Angela Koehler

Prof. Dr. Laurenz Thomsen

Dr. Silke Thoms

Dr. Bjoern Rost

Prof. Dr. Dieter Wolf-Gladrow

Date of defense: 29.01.2010

Alfred-Wegener-Institute for Polar and Marine Research

School of Engineering and Science – Jacobs University

List of contents

Publications

Publications

- Kaffes, A, Thoms S, Trimborn S, Rost B, Langer G, Richter K-U, Köhler A, Norici A, Giordano M. Carbon and nitrogen fluxes in the marine coccolithophore *Emiliania huxleyi* grown under different nitrate conditions, in preparation

Poster presentations

- Kaffes, A., Trimborn, S., Rost, B., Langer, G., Richter, K.-U., Norici, A., Giordano, M., Thoms, S. (2009). Effetcs of NO_3^- availability on carbon and nitrogen assimilation in the marine coccolithophore *Emiliania huxleyi*, 9th International Phycological Congress, Tokyo 2009, Japan.

Abstract

Coccolithophores are important primary producers and the most prolific calcifiers in the ocean. Since carbon (C) and nitrogen (N) assimilation are tightly connected, N availability has a crucial impact on photosynthesis and calcification, and therefore affects the biogeochemical function of coccolithophores in the sea. In general, N availability limits primary production in many areas in the ocean. Furthermore, N availability is expected to decrease in the near future, due to increased thermal stratification in the surface ocean and reduced nutrient input from deeper waters. Keeping this in mind, we examined the effects of NO_3^- availability on C and N assimilation in the marine coccolithophore *Emiliania huxleyi* under saturating light and present day pCO_2. Although growth rates and C to N ratios were similar in low and high NO_3^--grown cells, cellular organic C and N, and also inorganic C decreased under low NO_3^-. Growth at low NO_3^- caused a higher proportion of fixed C to be allocated to lipids relative to carbohydrates and proteins. Low NO_3^- availability led to downregulation of nitrate reductase (NR), nitrite reductase (NiR) and phosphoenolpyruvate carboxykinase (PEPCK) maximal activities (V_{max}), up-regulation of glutamine synthetase (GS) and glutamate synthase (GOGAT) V_{max}, and down-regulation of net photosynthesis and HCO_3^- uptake. The apparent Chl *α* specific efficiency of light harvesting (α) and CO_2 uptake remained similar, irrespective of the NO_3^- concentration in the culture medium. The affinity of NR for NO_3^-, NiR for NO_2^- and GS for Glu, as well as the affinities of inorganic C uptake were higher under low NO_3^-. This study suggests that maintenance of a constant C to N ratio under low and high NO_3^- requires a concerted regulation of the intracellular CO_2 and NO_3^- concentrations to equilibrate the fluxes through the C and N assimilation pathway.

List of selected abbreviations

α_{chl}	Apparent Chl *a* specific efficiency of light harvesting
Acetyl-CoA	Acetyl Coenzyme A
ADP	Adenosine phosphate
CA	Carbonic anhydrase
CCM	Carbon concentrating mechanism
Chl	Chlorophyll
Ci	Inorganic carbon
DIC	Dissolved inorganic carbon
EDTA	Ethylenediaminetetraacetic acid
Fer_{red}	Reduced ferredoxin
FTIR	Fourier transform infrared spectroscopy
Glu	Glutamate
Gln	Glutamine
GS	Glutamine synthetase
Gly	Glycine
GOGAT	Glutamate synthase

HEPES	4-(2-hydroxyethyl)-1-piperazineethanesulfonic acid
IR	Infrared
ICDH	Isocitrate dehydrogenase
kDa	Kilo Dalton
Km	Michaelis-Menten constant
LD	Light-dark
MDH	Malate dehydrogenase
mRNA	Messenger ribonucleic acid
NADPH	Nicotinamide adenine dinucleotide phosphate
NADH	Nicotinamide adenine dinucleotide
NiR	Nitrite reductase
NiT	Nitrite transporter
NR	Nitrate reductase
NT	Nitrate transporter
OAA	Oxalacetate
OG	Oxoglutarate
PDC	Pyruvate dehydrogenase complex
PEP	Phosphoenolpyruvate

PEPC	Phosphoenolpyruvate carboxylase
PEPCK	Phosphoenolpyruvate carboxykinase
PGA	Phosphoglycerate
PIC	Particulate inorganic carbon
POC	Particulate organic carbon
PON	Particulate organic nitrogen
RuBP	Ribulose bisphosphate
RubisCO	Ribulose bisphosphate carboxylase/oxygenase
Ser	Serine
TA	Total alkalinity
TCA	Tricarboxylic acid
TPC	Total particulate carbon
TrioseP	Triose phosphate
Vmax	Maximal activity

List of figures

List of tables

.

1. Introduction

1.1. The biogeochemical role of *Emiliania huxleyi* in the ocean

The marine coccolithophore *Emiliania huxleyi*, which is distributed worldwide except for the polar regions (Winter et al., 1994), is considered to be one of the major producers of calcite in the ocean (Baumann et al., 2004). Coccolithophores influence the carbonate pump by producing calcium carbonate, but as important marine primary producers, they also affect the organic carbon (C) pump through photosynthesis. The vertical transport of a part of the organic material produced via photosynthesis causes a drawdown of CO_2 in the surface ocean (organic C pump), whereas calcification displays an opposite role in the carbonate chemistry of the surface ocean by causing a net release of CO_2 during the formation and export of calcium carbonate (carbonate counter pump) (Fig. 1). The formation of calcite in the surface ocean and its sinking to deeper layers modifies the alkalinity of the upper water layer. The *rain ratio* represents the relationship of the particulate inorganic C to the particulate organic C in exported biogenic material, and may determine the biologically mediated CO_2 exchange between the surface ocean and the overlying atmosphere (Fig. 1).

Anthropogenic emissions increase the amount of CO_2 in the atmosphere, which in turn leads to changes in the seawater carbonate chemistry of the surface ocean (Fig. 2). The concentration of CO_2 increases in the surface ocean and as a consequence the carbonate ion (CO_3^{2-}) concentration and the pH decrease. An acidification of the upper ocean is already observed nowadays and is going to increase in the future (Fig. 2). Photosynthesis and calcification in *E. huxleyi* are sensitive to changes in the seawater carbonate chemistry (Rost et al., 2003; Iglesias-Rodriguez et al., 2008).

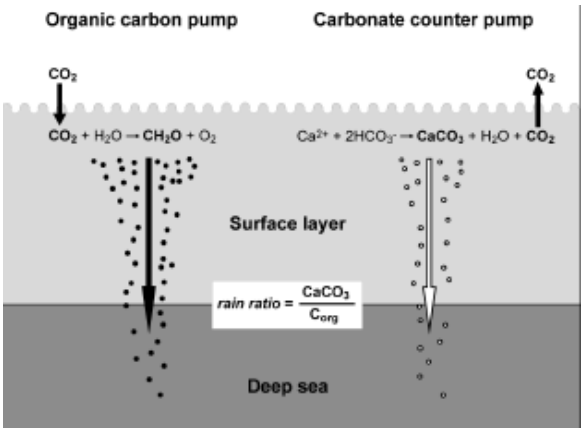

Figure 1. The biological carbon (C) pumps: Photosynthetic production of organic matter in the surface layer and its subsequent transport to depth (organic C pump), generates a CO_2 sink in the ocean. In contrast, calcium carbonate production and its transport to depth (carbonate counter pump), releases CO_2 in the surface layer. The relative strengths of these two processes (rain ratio) largely determine the biologically-mediated ocean atmosphere CO_2 exchange (in Rost and Riebesell, 2004).

The ongoing increase in atmospheric CO_2 affects the marine environment directly through changes in the seawater carbonate chemistry of the surface ocean and, indirectly through rising mean global temperatures (Intergovernmental Panel on Climate Change 2007). Increased temperatures in the surface ocean will increase thermal stratification and reduce therewith nutrient input from deeper waters, and will also have an impact on the light conditions of the upper water layer (Fig. 3).

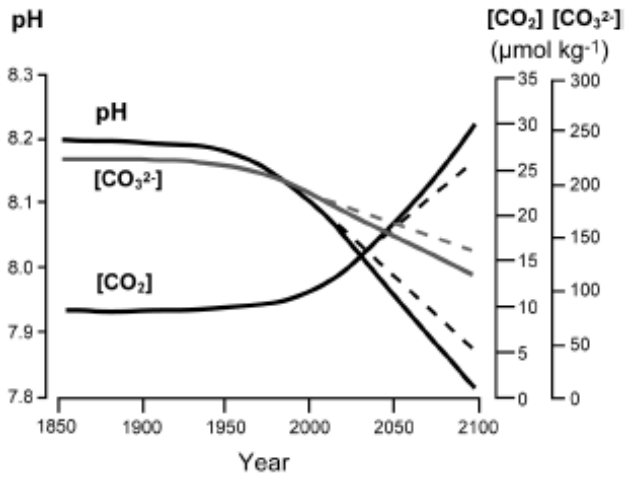

Figure 2. Seawater pH and the dissolved carbon dioxide (CO_2) and carbonate ion (CO_3^{2-}) concentrations in the surface layer of the ocean assuming a "business as usual" (IS92a) anthropogenic CO_2 emission scenario (Houghton et al., 1995). Dashed lines represent the predicted changes in carbonate chemistry if CO_2 emissions are reduced according to the Kyoto Protocol (in Rost and Riebesell, 2004; modified after Wolf-Gladrow et al., 1999).

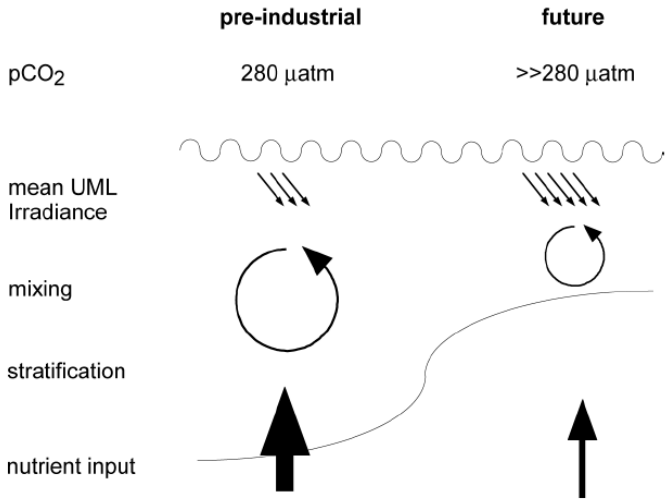

Figure 3. The progressive increase in atmospheric CO_2 affects the marine biota indirectly through rising mean global temperatures, thereby causing increased surface ocean stratification. This in turn reduces the nutrient input from deeper layers and increases the light availability due to shoaling of the upper mixed layer (in Rost and Riebesell, 2004).

1.2. Nitrogen-nitrate in the ocean

A high amount of the assimilated C in algae is devoted to N metabolism for the synthesis of proteins, nucleic acids and chlorophylls. Therefore the concentration and form of N in seawater should affect C assimilation in coccolithophores thereby altering their role in the global C cycle. Nitrogen can be found in the sea in form of inorganic and organic compounds (Sharp, 1975). Inorganic N includes molecular nitrogen (N_2), nitrate (NO_3^-), nitrite (NO_2^-), ammonium (NH_4^+), nitrous oxide (N_2O) and amine (NH_2). N_2 is by far the most abundant N compound (Tab. I), but can be utilized almost only by cyanobacteria in the ocean (Carpenter, 1975), and a small part by marine plants and their symbiotic bacteria (Capone, 1975). Besides N_2, NO_3^- is the most abundant species of inorganic N in the sea, whereas NO_2^- and NH_4^+ are less abundant altogether, but are of local significance (Tab. I). Organic N compounds (Williams, 1975), such as urea, amino acids, nucleic acids, nucleotides and nucleic bases contain both C, and N, may be also of great importance in certain areas in the sea (Tab. I).

Table I. Major nitrogen (N) species in the sea. Approximate average values are given for oceanic waters and appropriate ranges are given for coastal and estuarine waters.

All values are listed in µg atom N L^{-1} (in Sharp, 1983).

Species	Surface oceanic (0–100 m)	Deep oceanic (›100 m)	Coastal	Estuarine
Nitrogen gas N_2	800	1150	700-1100	700-1100
Nitrate NO_3^-	0.2	35	0-30	0-350
Nitrite NO_2^-	0.1	‹0.1	0-2	0-30
Ammonium NH_4^+	‹0.5	‹0.1	0-25	0-600
Dissolved organic N	5	3	3-10	5-150
Particulate organic N	0.4	‹0.1	0.1-2	1-100

In many areas in the sea, N limitation limits primary production (Dugdale, 1967; Howarth, 1988). As being one of the most common forms of inorganic N, NO_3^- plays a crucial role in marine primary productivity (Dugdale and Göring, 1967; Kanda, 1995). Nitrate concentrations vary in the ocean (Tab. I) with low NO_3^- concentrations (~ 5 nmol L^{-1}) in oligotrophic areas and higher NO_3^- concentrations (~ 30 µmol L^{-1}) in upwelling systems, as reported by Rees et al. (2006) for the Atlantic Ocean. Although, *E. huxleyi* is capable of utilizing also dissolved organic N (Ietswaart et al., 1994; Palenik and Henson, 1997), NO_3^- is an important N source for the growth of this coccolithophore (Page et al., 1999).

1.3. Nitrate assimilation

Nitrate assimilation includes NO_3^- transport into the cell, the cytosolic reduction of NO_3^- to NO_2^-, the NO_2^- transport into the chloroplast and its subsequent reduction to NH_4^+ (Fig. 4). Ammonium is then incorporated into C skeletons in the chloroplast or the cytosol (Fig. 5). Nitrate assimilation by marine phytoplankton has been studied, either by measuring the reduction in NO_3^- concentration in the culture medium (Dortch et al., 1982) or the incorporation of NO_3^- containing the isotope ^{15}N in algal biomass (Lomas and Glibert, 2000).

The transport of NO_3^- into the cell is mediated by NO_3^- transporter(s) (Nrt(s)) in the plasma membrane (Fig. 4) and it was suggested to be a key step controlling the amount of NO_3^- assimilated by cells (Galvan and Fernandez, 2001). Four different gene systems (*Nrt2.1/Nar2, Nrt2.2/Nar2, Nrt2.3, Nrt2.X*) are responsible for NO_3^- transport, and some of them also for NO_2^- transport, in *Chlamydomonas reinhardtii* (Quesada et al., 1994; Quesada and Fernandez, 1994; Galvan et al., 1996; Rexach et al., 1999; Fernandez and Galvan, 2007). These NO_3^- transport systems can be distinguished in high and low affinity NO_3^- transporters. Apart from one NO_3^- transporter which is constitutively expressed in *C. reinhardtii*, NO_3^- was found to

induce the expression of all other NO_3^- transport systems, whereas NH_4^+ represses them (Galvan et al., 1996; Rexach et al., 1999). High-affinity NO_3^- transporter genes (*Nrt2*) have been described in *E. huxleyi* and *Nrt2* gene transcripts were found to be induced in the presence of NO_3^-, but also under N starvation (Song and Ward, 2007).

Nitrate reductase (NR) is the first enzyme in the NO_3^- reduction pathway and is located in the cytosol (Fig. 4). NR catalyzes the two electron reduction of NO_3^- to NO_2^-. The energy for this reductive step is supplied by the oxidation of NADH/NADPH. Although characterization of the gene coding for NR is still missing in *E. huxleyi*, the molecular mass and kinetics of the purified NR enzyme have been recently described in this phytoplankton species (Iwamoto and Shiraiwa, 2003). Native *E. huxleyi* NR has an overall mass of 514 kDa and is composed of six 85 kDa homologous subunits (Iwamoto and Shiraiwa, 2003). The K_m for NADH and NO_3^- of purified NR were 40 µM and 104 µM, respectively (Iwamoto and Shiraiwa, 2003). Nitrate seems to play an important role in regulating NR gene and protein expression, as well as NR activity. Nitrate acts positive on NR mRNA and protein expression in *C. reinhardtii* (Navarro et al., 1996). Furthermore, increasing NO_3^- concentrations were found to increase NR activity in the marine diatom *Thallassiosira pseudonana* (Berges and Harrison, 1995) as well as in the green algae *Dunaliella primolecta* and *Chlorella stigmatophora* (Hipkin et al., 1983). NR seems to be of great importance in the NO_3^- assimilation pathway through its involvement in the regulation of the NO_3^-/NO_2^- transport as reported for *C. reinhardtii* cells (Navarro et al., 1996).

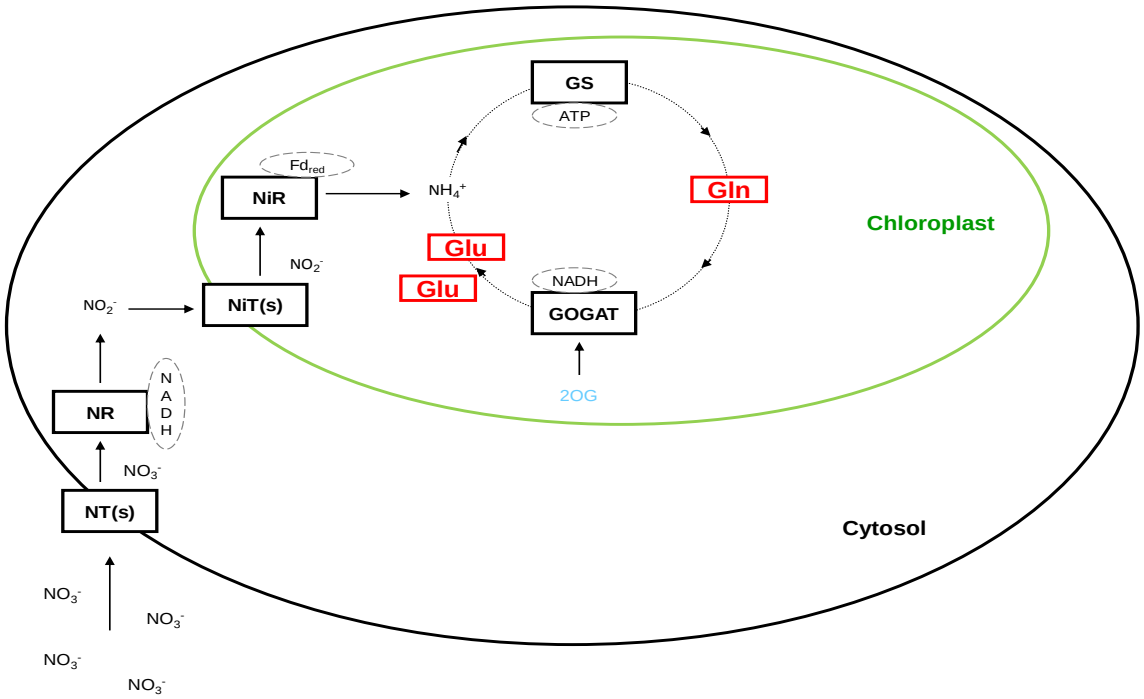

Figure 4. The nitrate (NO_3^-) assimilation pathway including NO_3^- reduction to NH_4^+ and incorporation of NH_4^+ into C skeletons in the chloroplast. NT: nitrate transporter; NR: nitrate reductase; NiT: nitrite transporter; NiR: nitrite reductase; NH_4^+: ammonium; GS: glutamine synthetase; GOGAT: glutamate synthase ATP: adenosine triphosphate; NADH: nicotinamide adenine dinucleotide; Fer_{red}: reduced Ferredoxin; Glu: glutamate; Gln: glutamine and 2OG: 2 oxoglutarate.

The transport of NO_2^- into the chloroplast is mediated via NO_2^- transporters in the chloroplast envelope (Fig. 4). Nitrite transporters have not been studied yet in *E. huxleyi* neither at the gene nor at the protein level. Two high-affinity NO_2^- transporters have been identified in *C. reinhardtii* and their expression was found to be induced by NO_3^- and repressed by NH_4^+ (Rexach et al., 1999). Rexach et al. (2000) reported the existence of the *Nar1* gene which codes for a transmembrane protein (NAR1) involved in the transport of NO_2^- from the cytosol into the chloroplast. This protein was found to be essential for growth under NO_3^- limiting conditions and seems to control the amount of NO_3^- incorporated under limiting CO_2

conditions (Rexach et al., 2000). Galvan et al. (2002) have reported the existence of various *Nar1* genes involved in NO_2^- transport and Mariscal et al. (2006) showed that the *Nar1* gene family is differentially regulated in response to the C and N source.

Nitrite is reduced to NH_4^+ in the chloroplast and the reaction is catalyzed by the NiR which utilizes reduced ferredoxin. As in the case of NO_2^- transporters, the NiR enzyme has not been studied yet in the coccolithophore *E. huxleyi*. Maximal activity of NiR in *C. reinhardtii* was detectable only in the presence of NO_3^- and NH_4^+ was found to repress NiR activity (Galvan et al., 1991). The gene *Nii1* coding for NiR in *C. reinhardtii* was found to be located in the same gene cluster with other NO_3^- assimilating genes and it was found to be regulated in response to light and N availability (Quesada et al., 1998). The kinetics of NR and NiR as well as optimal temperature of NR and NiR activities were studied in diatoms and flagellates by Lomas and Glibert (2000). The authors suggested that differences in the affinity of NR for NO_3^- and the temperature optimum of NR activity may in part explain the timing of the occurrence of diatom and flagellate blooms.

Ammonium is incorporated into C skeletons mainly via the GS/GOGAT cycle (Lea et al., 1990), which is located in both chloroplast (Fig. 4) and cytosol (Fig.5). The GS/GOGAT cycle produces glutamine (Gln) and glutamate (Glu), which are the starting compounds for the synthesis of all rest amino acids, nucleic acids and chlorophylls (Fig. 6). Two GS isoenzymes, a cytosolic (GS_1) and chloroplastic (GS_2) one, have been identified in *E. huxleyi* (Maurin and Le Gal, 1997). Both isoforms are homohexamers with molecular masses of 402 kDa for $GS_1$and 501 kDa for GS_2, whereas the molecular masses of the subunits of GS_1 and GS_2 were estimated to be 61 and 70 kDa, respectively (Maurin and Le Gal, 1997a). The same authors reported that the K_m for hydroxylamine (NH_2OH) was approximately 3 mM for both

GS isoforms, but GS_2 had higher affinity for Gln than GS_1. The genes coding for the GS and GOGAT enzymes have not been studied yet in *E. huxleyi*, and in the case of GOGAT no data is available for the expression pattern of the protein and its activity. Decreasing NO_3^- concentrations were found to stimulate GS and GOGAT activity in various phytoplankton cells (Tischner and Hüttermann, 1980; Menacho and Vega, 1989; Maurin and Le Gal, 1997b) and to increase the affinity of GS for NH_4^+ in *E. huxleyi* (Maurin and Le Gal, 1997b). GS activity was also found to exhibit a marked diel periodicity in *E. huxleyi* with maximal values during the dark period and a minimum during the light period (Maurin-Defossez and Le Gal, 1998).

1.4. Carbon skeletons for amino acid synthesis

The C skeletons for amino acid synthesis in the GS/GOGAT cycle are mainly provided via the tricarboxylic acid (TCA) cycle (Elfiri and Turpin, 1986; Weger and Turpin, 1989) (Fig. 7). The removal of intermediates of the TCA cycle requires that the cycle is replenished of its intermediates via anaplerotic reactions (Beardall and Raven, 1990; Norici and Giordano, 2002). Furthermore, the provision of inorganic carbon (Ci) for these reactions may be crucial to sustain amino acid and protein synthesis (Norici and Giordano, 2002). Tsuji et al. (2009) reported that β-carboxylases including phosphoenolpyruvate carboxykinase (PEPCK) contribute to the anaplerotic reaction by providing C skeletons for amino acid and lipid synthesis. Although the exact role of β-carboxylases in response to N availability has not been

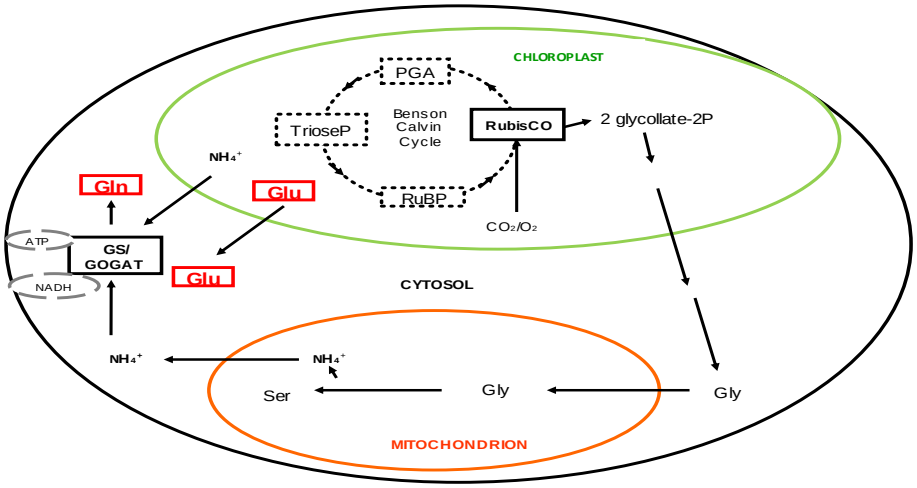

Figure 5. Cytosolic ammonium assimilation. NH_4^+: ammonium; GS: glutamine synthetase; ATP: adenine triphosphate; NADH: nicotinamine adenine dinucleotide; Glu: glutamate; Gln: glutamine; RubisCO: ribulose bisphosphate carboxylase/oxygenase; RuBP: ribulose bisphosphate; Gly: glycine; Ser: serin; PGA: phosphoglycerate: TrioseP: triose phosphate.

studied yet in *E. huxleyi*, NO_3^- supply to N limited *Selenastrum minutum* led to increased β-carboxylase activities in this species (Elfiri and Turpin, 1987). Furthermore, Norici et al. (2002) reported that the expression of phosphoenolpyruvate carboxylase (PEPC) isoforms in *Dunaliella salina* responds to the variation in the C skeleton demand deriving from changes in the chemical form and availability of N. In general, the capacity for N assimilation increases in cells under N limitation, as reported for N limited cells of *Selenastrum minutum* (Birch et al., 1986; Elfiri and Turpin, 1986).

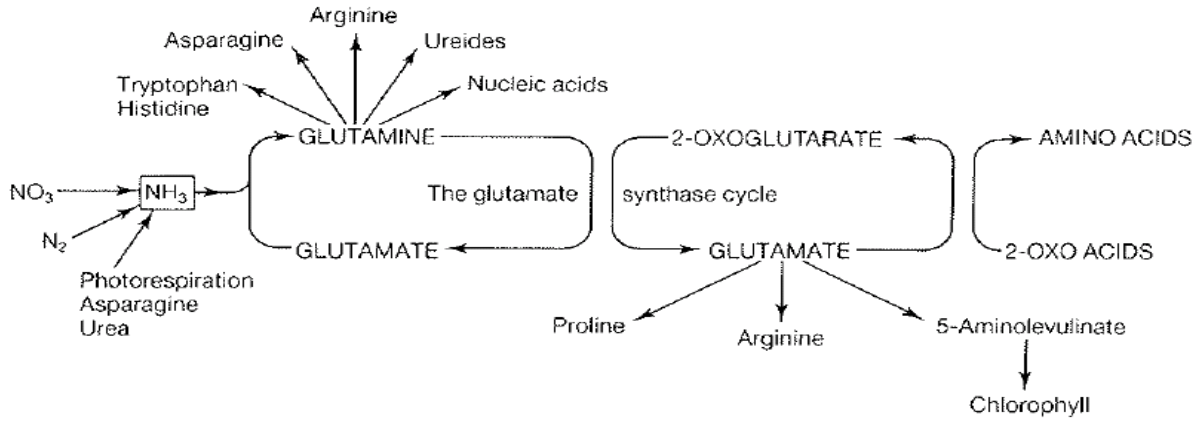

Figure 6. The GS/GOGAT cycle produces glutamine and glutamate which are the starting compounds for the synthesis of all remaining amino acids, nucleic acids and chlorophylls (Lea et al., 1993).

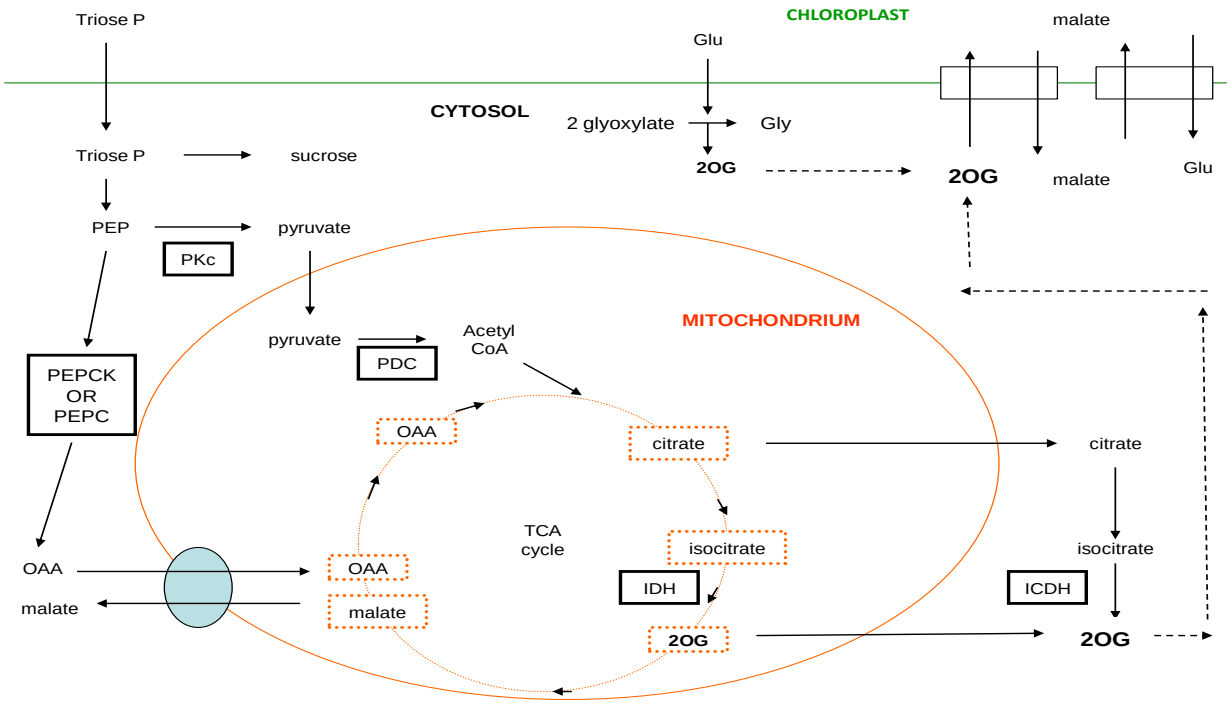

Figure 7. The C skeletons needed for amino acid synthesis are mainly provided via the TCA cycle in form of 2-oxoglutarate (2OG). PEPCK: phosphoenolpyruvate carboxykinase; PEPC: phosphoenolpyruvate carboxylase; PKc: pyruvate kinase C; PDC: pyruvate dehydrogenase complex; ICDH: isocitrate dehydrogenase; Glu: glutamate; Gly: glycine; TrioseP: triose phosphate; OAA: oxalacetate; Acetyl-CoA: acetyl coenzyme A, PEP: phosphoenolpyruvate.

1.5. Inorganic carbon assimilation

The inorganic C (Ci) acquisition has been suggested to play an important role in the evolution and ecology of marine phytoplankton (Badger et al., 1998**;** Tortell, 2000; Giordano et al., 2005). The main carboxylating enzyme, ribulose1,5-bisphosphate carboxylase/oxygenase (RubisCO) is characterized by a low affinity for its substrate and microalgae cells have to invest an important amount of energy in order to enhance CO_2 concentration in the carboxylation site of RubisCO and avoid Ci limitation (Badger et al., 1998). Therefore, cells have developed special mechanisms, i.e. carbon concentrating mechanisms (CCMs), including the active uptake of CO_2 or HCO_3^- or both as well as the enzyme carbonic anhydrase (CA), which accelerates the otherwise slow conversion rate between HCO_3^- and CO_2 (Fig. 8). The β-carboxylase PEPC may also contribute, together with active HCO_3^- uptake, to the CCM as reported for diatoms (C_4-like pathway) (Reinfelder et al., 2000, 2004). The effects of N availability on the regulation of the CCM have still to be studied in *E. huxleyi*. Nevertheless, the CCM of this species was found to be regulated in response to light and CO_2 (Rost et al., 2003; Rost et al., 2006; Trimborn et al., 2007). In general, the CCMs have been suggested to improve N-use efficiency in microalgae, mainly by increasing the achieved rate of CO_2 fixation per unit N in Rubisco (Raven, 1997; Beardall et al., 1998), thereby controlling the cellular elemental ratios, specifically the C to N ratio (Beardall and Giordano, 2002).

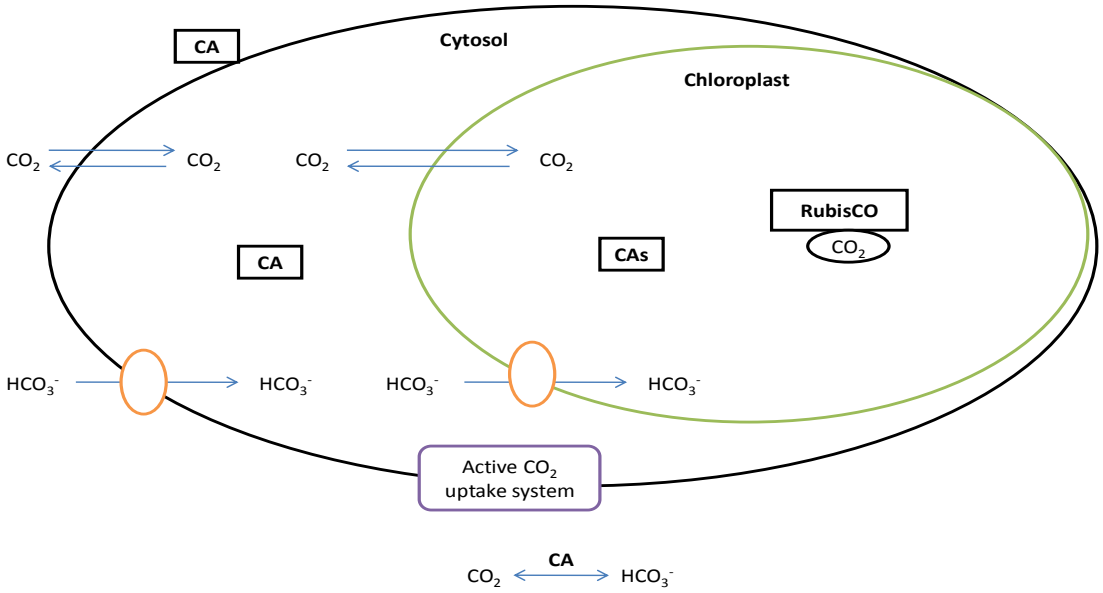

Figure 8. Carbon concentrating mechanisms (CCMs) in eukaryotic algal cells. Bicarbonate (HCO_3^-) is taken up by specific HCO_3^- transporters, whereas CO_2 is mainly taken up by diffusion. An active CO_2 system seems to exist, but it is poorly described till now. The enzyme carbonic anhydrase (CA) catalyzes the conversion between CO_2 and HCO_3^-. Various isoenzymes of CA have been described, which are located in the chloroplast stroma, the thylakoid membrane, the cytosol, the mitochondrium (not shown here) and the extracellular space. RubisCO: ribulose bisphosphate carboxylase/oxygenase.

1.6. Photosynthesis and respiration

In photosynthetic organisms, all ATP and reductant (NADH/NADPH) come from photosynthesis directly through the light-dependent reactions or indirectly through respiration of fixed C and this enables cells to afford the energy requirements of C and N assimilation (Tab. II). Nitrogen limitation was found to decrease the rate of photosynthesis in the diatom *Phaeodactylum tricornutum* (Osborne and Geider, 1986). The most obvious effect, which causes the decrease in photosynthesis under N limitation, is the decline in nitrogenous

photosynthetic pigments such as chlorophylls (Chl) and phycobilins (Falkowski et al., 1989; Herzig and Falkowski, 1989; Plumley et al., 1989). Furthermore, the carotenoid to chl α ratio increases dramatically under N limitation (Plumley et al., 1989). Nitrogen limitation also decreases thylakoid stacking and absorptivity (Rhiel et al, 1985, 1986). Interestingly, N limitation was found to increase, decrease or maintain the apparent Chl specific efficiency of light harvesting (α_{chl}), depending on the investigated organism and the degree of N limitation (Osborne and Geider, 1986; Kolber et al., 1988; Herzig and Falkowski, 1989)**.** Similarly to photosynthetic pigments, the enzymes of photosynthetic C fixation are also affected under N limitation and a decline in RubisCO per cell was reported in previous studies (Lapointe and Duke, 1984; Falkowski et al., 1989; Beardall et al., 1991). Respiration was shown to support NO_3^- and NO_2^- reduction during photosynthesis in *S. minutum* (Weger and Turpin, 1989). The impact of N availability on photosynthesis and respiration has still to be tested in the marine coccolithophore *E. huxleyi*.

1.7. Effects of nitrogen limitation on *Emiliania huxleyi*

The effect of NO_3^- availability on C and N assimilation in *E. huxleyi* cells was the subject of several studies in the past (Paasche, 1998; Fritz, 1999; Riegmann et al., 2000). Cellular particulate organic C (POC) and N (PON) have been shown to decrease with increasing NO_3^- limitation (Riegmann et al., 2000). According to Riegmann et al. (2000), various levels of N limitation did not have any influence on cellular inorganic C (PIC) but cellular PIC production decreased due to decreasing growth rate. In contrast, cellular PIC was found to increase with increasing NO_3^- limitation in cyclostat cultures (Fritz, 1999). Moreover, *E. huxleyi* cells were covered by multiple layers of coccoliths at low NO_3^- concentrations (Lindschooten et al., 1991; Fritz, 1999). Nitrate limitation has also been shown to decrease the calcite content of coccoliths (Paasche et al., 1998).

Table II. The energetics of CO_2 and N assimilation (simplified). Table I outlines the ATP and reductant requirements of the various processes associated with photosynthetic C fixation and the assimilation of N into protein (in Turpin, 1991).

The equations are not balanced.

Process	Reactions	ATP/e^- requirement
1. Photosynthetic CO_2 fixation	CO_2 + RuBP + 3ATP + $4e^-$ → RuBP + 1/3 triose-P	0.75
2. N transport	N_{out} + ATP → N_{in}	
3. NO_3^- reduction (NR)	NO_3^- + $2e^-$ → NO_2^-	
4. NO_2^- reduction (NiR)	NO_2^- + $6e^-$ → NH_4^+	
5. NH_4^+ assimilation (GS/GOGAT)	NH_4^+ + Glu + α-KG + ATP + $2e^-$ → 2Glu	
6. Amino acid interconversion (transaminase)	Glu + keto-acid → amino acid + 2-OG	
7. Protein synthesis	Amino acid + 4ATP → polypeptide	
8. NO_3^- assimilation into protein (2 + 3 + 4 + 5 + 7)	NO_3^- + keto-acid + 6ATP + $10e^-$ → protein	0.6
9. NO_2^- assimilation into protein (2 + 4 + 5 + 7)	NO_2^- + keto-acid + 6ATP + $8e^-$ → protein	0.75
10. NH_4^+ assimilation into protein (2 + 5 + 7)	NH_4^+ + keto-acid + 6ATP + $2e^-$ → protein	3

1.8. Objectives of the study

Although biochemical studies have been conducted on sole proteins such as NR (Iwamoto and Shiraiwa, 2003) and GS (Maurin and Le Gal, 1997) in *E. huxleyi*, knowledge on the effect of NO_3^- availability on the kinetics of inorganic C/N acquisition and assimilation is still lacking for this common phytoplankton species. The main goal of this study is to describe the C and N fluxes from the cellular to the environmental level, with starting point the intracellular processes involved in C/N metabolism and end point the elemental ratios which define the impact of the species on its environment. Therefore the regulation of NR and NiR kinetics which describe the capacity of the NO_3^- to NH_4^+ reduction pathway is investigated in response to NO_3^- availability. Ammonium assimilation into C skeletons via the GS/GOGAT cycle is studied by measuring the kinetics of GS and GOGAT activity, but also through determination of the GS isoforms in *E. huxleyi* cells grown under different NO_3^- conditions. The acquisition of inorganic C in cells is investigated via the kinetics of CO_2 and HCO_3^- uptake in response to NO_3^- availability. The impact of the NO_3^- concentration in the culture medium on photosynthesis, respiration and allocation of fixed C into the macromolecular pools is also studied in cells of *E. huxleyi*. Furthermore the elemental composition of cells, and especially cellular organic C and N as well as inorganic N, is also determined in cells grown at different NO_3^- conditions. Finally, the intracellular NO_3^- and CO_2 concentrations in the active sites of NR and RubisCO needed for adequate cellular growth are calculated in *E. huxleyi* cells in response to NO_3^- availability. With all these measurements, the hypotheses whether cellular C and N fluxes require a controlled regulation in response to NO_3^- availability and whether different NO_3^- conditions have an impact on the allocation of the macromolecular pools and growth in *E. huxleyi* cells are tested.

2. Materials and methods

2.1. Culture conditions

The coccolith-bearing strain B 92/11 (J. C. Green 1990, Plymouth Marine Laboratory) of *E. huxleyi* was grown in semi continuous cultures in 10-L polycarbonate flasks. Experiments were carried out under 16:8 h light-dark (LD) cycle at a constant temperature of 15°C. The applied mean photon flux density was 240 µmol photons m^{-2} s^{-1}. The culture flasks were aerated with air containing CO_2 partial pressure (pCO_2) of 37.5 Pa and placed on a shaker, to keep the cells in suspension. The growth medium was prepared from sterile-filtered (0.2 µm pore-size cellulose-acetate filters, Sartorius) natural seawater. Nutrient additions, with the exception of iron and NO_3^-, were made according to the f/2 recipe (Guillard and Ryther, 1962). The iron concentration in the culture medium was 8 nM and was sufficient to cover the iron need of the relative low cell densities in our experiment, as determined in preliminary experiments. The initial NO_3^- concentrations in the growth medium were ca. 280 µM in the high and ca. 10 µM in the low NO_3^- treatment. Over the course of the experiment, cell densities were kept between $3 * 10^4$ and $3 * 10^5$ cells mL^{-1} by regular dilutions. This dilution pattern was kept throughout the whole experiment, which lasted 1 year. The cells were acclimated to the experimental conditions for approximately 2 weeks before measurements. Growth rates were calculated from daily cell counts by means of a cell counter (COULTER MULTISIZER 3, Beckmann).

2.2. Carbonate chemistry

Samples for total alkalinity (TA) measurements were filtered (nominal pore size 0.6 µm GFF filters, Whatman), and the filtrate was stored at 4°C and measured by means of potentiometric

titration with an average precision of ± 8 µeq kg^{-1} (Brewer et al., 1986). TA was calculated from linear Gran plots (Gran, 1952). Samples for dissolved inorganic carbon (DIC) were sterile-filtered (0.2 µm pore size cellulose-acetate syringe filters, Sartorius, Göttingen, Germany) and stored free of air bubbles at 4°C until they were measured with an average precision of ± 10 µmol kg^{-1} (QUAATRO, Seal Analytical). Values for pCO_2 were calculated using the program CO_2sys (Lewis and Wallace, 1998). Equilibrium constants of Mehrbach et al. (1973) refitted by Dickson and Millero (1987) were chosen.

2.3. Cellular carbon and nitrogen

Samples for total particulate C (TPC), POC and PON were filtered onto precombusted (500°C, 12 h) filters (nominal pore size 0.6 µm GFF filters, Whatman) and stored in precombusted (500°C, 12 h) petri-dishes at -20°C. Filters for POC were treated before analysis with 200 µl HCl (0.1 M) to remove all inorganic C. TPC, POC and PON samples were measured on an elemental analyzer mass spectrometer (ANCA-SL 2020, Secron). Values for PIC were calculated as the difference between TPC and POC. POC, PON and PIC production was measured by multiplying the cellular POC, PON and PIC content with the growth rate.

2.4. Macromolecular composition

Cells for fourier transform infrared spectroscopy (FTIR) analyses were harvested by centrifugation at 1500 x g for 15 minutes and washed twice with an isoosmotic solution of ammonium formate, to minimize the carry-over of IR absorbing medium components. Cells were resuspended in ammonium to obtain the concentration that was preliminary determined to afford the best signal to noise ratio. Aliquotes of 50 µL of these suspensions were deposited on silica windows (Crystran Ltd., Poole, UK) and desiccated in an oven at 60°C for at least 3

hours. Silica windows on which 50 µL of ammonium formate solution were deposited were treated as the samples and used as blanks (Domenighini and Giordano, 2009).

FTIR spectra were acquired with a Tensor 27 FTIR spectrometer (Bruker Optics, Ettlingen, Germany) as described in Domenighini and Giordano (2009). All spectra were baseline corrected prior to any analysis applying the Rubberband correction function of the OPUS 6.0 software (Bruker Optics, Ettlingen, Germany) and then normalized to the amide I band (~1650 cm^{-1}). Bands were assigned to the macromolecular pools according to Giordano et al. 2001. The sum of the integrals of the absorption bands at ~1160 cm^{-1}, ~1080 cm^{-1} and ~1030 cm^{-1} was used as a proxy for carbohydrates. The amide I peak (1650 cm^{-1}) was used as an indicator of protein relative abundance. The ~1740 cm^{-1} feature was used for lipids. Relative ratios of protein, carbohydrates and lipids were calculated from the bands' integrals, using the OPUS 6.5 software (Bruker Optik GmbH, Ettlingen, Germany). The calculation of the band integrals was performed after deconvolution of the spectrum from 1800 cm^{-1} to 1000 cm^{-1} using the Peak fit function of OPUS 6.5; to minimize subjective assessments, the main peaks on which deconvolution was based were identified by the application to each spectrum of a second derivative, with 9 smoothing points.

2.5. Coccolith morphology

Samples for scanning electron microscope analysis were filtered on polycarbonate filters (0.2 µm pore size, Whatman), dried in a drying cabinet at 60°C for 24 hours, then sputter-coated with gold-palladium. Imaging was performed with a digital scanning field-emission electron microscope (XL-30, Philips). Four categories were used to describe the morphology of *E. huxleyi* coccoliths: 'normal', 'malformed', 'incomplete', and 'incomplete and malformed'. An

average of approx. 350 coccoliths was analyzed per sample. For determination of the number of visible coccoliths per cell an average of approx. 50 cells per sample was counted.

2.6. Enzyme extraction

The cells were sampled about 4 hours after the beginning of the light period. Cells were concentrated by centrifugation at 2,772 *g* for 6 min at 4°C (Megafuge 1.0 R, Heraeus), frozen in liquid N_2 and stored at – 80°C. The cells were gently disrupted using a hand operated glass homogenizer (Wheatman) at 4°C. All extracts were centrifuged at 16,060 *g* for 15 min at 4°C (Biofuge fresco, Heraeus), in order to spin down the calcite. The supernatant was centrifuged again at 61,740 g for 20 min at 4°C (OPTIMA^{TM} LE-80K Ultracentrifuge, Beckmann). The resulting supernatant was used to study enzyme kinetics and measure total protein amount. The protein amount in extracts was measured according to the method of Bradford (1976), using BSA as standard. All solutions were made in Milli-Q H_2O (Milli-Q academic A10, Millipore) and the chemicals were purchased by Sigma-Aldrich (St. Louis, MO, USA).

2.7. Nitrate reductase

Nitrate reductase activity was determined by NO_3^- reduction to NO_2^- and subsequent colorimetric measurement of the NO_2^- produced according to the method described by Giordano et al. (2005b). The extraction buffer for NR (buffer A) contained 50 mM HEPES (pH 7.5), 1 mM EDTA, 1 mM dithiothreitol, 0.1% Triton X-100 (v/v), 0.3% polyvinylpolypyrrolidone (w/v) and 10 mM $MgSO_4$. The amount of NO_2^- was measured according to the method of Snell and Snell (1949) in a microplate reader (SPECTRAFLUOR, Tecan) at 535 nm. Controls included the same reaction mixture, but extraction buffer was used instead of extract. The amount of NO_2^- in the tubes was quantified according to a NO_2^-

standard curve from 0 to 40 µM. Nitrate concentrations from 0.005 to 20 mM and NADH concentrations from 5 to 400 µM were used for the determination of NR kinetic parameters.

2.8. Nitrite reductase

Activities of NiR were determined using an assay similar to Wray and Filner (1970), which is based on the colorimetric measurement of the NO_2^- left in the reaction mixture. Buffer A was used for NiR extraction and the reaction was run in open tubes. The assay mixture contained in a total volume of 500 µL: 100 µL of 150 mM phosphate buffer (pH 7.5), 20 µL Milli-Q H_2O, 250 µL of 32 mM $NaNO_2$, 5 µL of a 100 mM methyl viologen solution, 50 µL of extract and 75 µL of fresh $Na_2S_2O_4$ (25 mg mL^{-1} $Na_2S_2O_4$ in 0.29 M $NaHCO_3$) solution. The reaction mixture was incubated for 15 min at 30°C and was initiated by adding the sodium dithionite solution. The reaction was stopped by vigorous shaking until the dithionite was completely oxidized and the solution turned from dark blue to colourless. Controls included the same reaction mixture, but extraction buffer was used instead of extract. The amount of NO_2^- was measured in a microplate reader at 535 nm according to the method of Snell and Snell (1949) with a standard curve from 0 to 40 µM NO_2^-. Nitrite concentrations from 0.25 to 16 mM were used in the assay, in order to determine the NiR kinetic parameters.

2.9. Glutamine synthetase

Glutamine synthetase activity was determined from the formation of L-Glu γ-monohydroxamate as described by O'Neal and Joy (1973), and Oaks et al (1980). The extraction buffer for GS (buffer B) contained 50 mM HEPES (pH 7.5), 1 mM EDTA, 2 mM dithiothreitol, 0.1% Triton X-100 (v/v), 0.3% polyvinylpolypyrrolidone (w/v) and 10 mM $MgSO_4$. The extracts were desalted by applying them on a Sephadex column (PD-10

DESALTING COLUMN, GE Healthcare, Uppsala, Sweden). The extracts were eluted using 50 mM HEPES (pH 7.5). An assay mixture containing 160 mM HEPES (pH 7.5), 4.8 mM hydroxylamine (pH 7.5), 3.2 mM $MgSO_4$ and 0.16 mM EDTA was prepared. The reaction was conducted in a 96-well plate in a final volume of 200 µL. To a 76.4 µl aliquot of the assay mixture, we added 25.6 µL of 6.25 mM ATP (pH 7.5) and 76.8 µL extract. The reactants were incubated for 5 min at 30°C. At last, 21.2 µL of 0.6 M Glu were added, the microplate was incubated for 20 min at 30°C. The reaction was terminated by adding 40 µL of a $FeCl_3$ solution [2.5% $FeCl_3$ (w/v), 5% TCA (w/v), 1.5 N HCl]. The reactants were centrifuged at 16,060 g for 2 min. Controls were run, in which 50 mM HEPES (pH 7.5) was used instead of extract. A second control was run, in which the reaction was stopped by adding the $FeCl_3$ solution immediately after the Glu addition. The amount of L-Glu γ-monohydroxamate was measured in a microplate reader at 535 nm with a standard curve from 0 to 25 µM γ-L-Glu monohydroxamate. Glu concentrations from 0.5 to 63.6 mM, ATP concentrations from 0.025 to 3.2 mM and hydroxylamine concentrations from 0.02 to 4.8 mM were used to derive GS kinetic parameters.

The maximal enzyme activity (V_{max}) and the Michaelis-Menten constant (K_m) for NR, NiR and GS were calculated from the Michaelis-Menten equation

$$Vo = \frac{Vmax[S]}{Km + [S]}$$

where Vo is the enzyme activity, V_{max} is the maximum enzyme activity, [S] is the substrate concentration and K_m is the Michaelis-Menten constant.

2.10. Glutamate synthase

Glutamate synthase activity was determined by the reduction in the absorbance of NADH similar to the methods of Singh and Srivastava (1986) and Lin and Kao (1996). Buffer A was used for GOGAT extraction. The assay mixture contained 125 mM HEPES (pH 7.5), 5 mM EDTA, 20 mM KCl and 875 µM NADH. The reaction was conducted in a 96-well plate in a final volume of 250 µL. To a 50 µl aliquot of the assay mixture, we added 100 µL extract, 50 µL of 20 mM Gln and 50 µL of 5 mM 2-oxoglutarate (2-OG). Controls included the same reaction mixture, in which the extract was substituted with extraction buffer. The reduction in NADH absorbance was measured for 2 min at 30 °C in a microplate reader (Spectrafluor, Tecan) at 340 nm, immediately after the addition of 2-OG.

2.11. Phosphoenolpyruvate carboxykinase

Phosphoenolpyruvate carboxykinase activity was determined through the coupled reaction with malate dehydrogenase (MDH), as described by Holsworth and Bruck (1977) and Johnston and Raven (1989). Buffer A, pH 7.9 was used for PEPCK extraction. The extracts were desalted by applying them onto a Sephadex column (PD-10 DESALTING COLUMN, GE Healthcare, Uppsala, Sweden) and proteins were eluted using 50 mM HEPES (pH 7.9). The assay mixture had the following composition: 50 mM HEPES (pH 7.9), 10 mM $NaHCO_3$, 5 mM dithiothreitol, 200 µM NADH and MDH (1 µL mL^{-1} assay mixture). To 100 µl extract, we added 67.75 µL assay mixture, 12.5 µL of 100 mM phosphoenolpyruvate, 25 µL of 100 mM $MgCl_2$, 12.5 µL of 10 mM ADP and 32.25 µL Milli-Q H_2O. PEPCK activity was measured from the rate of reduction of NADH absorbance for 60 min, at 30 °C, in a microplate reader (Spectrafluor, Tecan) at 340 nm. Two controls were run; one included Mn instead of Mg, the other contained Milli-Q H_2O instead of ADP. We did not measure PEPC

activity, because it was found to be one order of magnitude lower than PEPC activity in *E. huxleyi* strain PML 92/11 (data not shown).

2.12. Purification of the glutamine synthetase isoforms

We also verified whether different GS isoforms existed in *E. huxleyi* and if their relative amount was dependent on the growth NO_3^- concentration. The purification of GS isoforms was conducted by means of HPLC (Jasco PU-1580/LG-1580-04/DG-1580-54/MD-2010-plus/AS-1555/CO-1560, Jasco, Groß-Umstadt, Germany), similar to the GS purification procedure described in Maurin and Le Gal (1997a). Proteins were separated due to their molecular size, affinity to adenylates and charge. All solutions used during the purification procedure were air-free and each purification step was conducted at 4 °C. Proteins were extracted in buffer (B) at 4 °C. The crude extracts were desalted and proteins were concentrated by means of ultracentrifugation to a final volume of 200 µL (AMICON ULTRA CENTRIFUGAL FILTER UNITS, Sigma-Aldrich, St. Luis, MO, USA). The protein aliquots (3.5 and 3.6 mg mL^{-1} for high and low NO_3^--grown cells, respectively) were initially run through a Sephacryl S-200 HR column (GE Healthcare, Uppsala, Sweden). The proteins were eluted with in HEPES [50 mM, pH 7.5) and fractions were collected at a flow rate of 1 mL min^{-1}. Detection of proteins was performed at 280 nm and two GS active fractions were detected. The GS active fractions were concentrated by ultrafiltration to a final volume of 200 µL. One aliquot was used for estimating GS activity, the rest was applied in a HiTrap Blue HP 1 mL column (GE Healthcare, Uppsala, Sweden) and eluted with buffer HEPES [50 mM, pH 7.5) at a flow rate of 1 mL min^{-1}. The active GS fractions were concentrated by ultracentrifugation to a final volume of 200 µL. One aliquot was used for estimating GS activity, the rest was applied to a MonoQ 5/50 GL column (GE Healthcare, Uppsala, Sweden) and proteins were fractionated using a linear salt gradient of 0-500 mM NaCl in buffer

HEPES (50 mM, pH 7.5) with a flow rate of 1 mL min^{-1}. At the end of the purification, aliquots of the GS active fractions were loaded on a 10% SDS-PAGE gel (Laemmli, 1970) and proteins were silver stained (SILVER STAIN KIT, Biorad).

2.13. Photosynthesis and inorganic carbon fluxes

Inorganic carbon (Ci) fluxes during steady-state photosynthesis were investigated by means of a sector-field multicollector mass spectrometer (ISOPRIME, GV Instruments, Manchester, UK**)**. Net photosynthesis was measured by monitoring the O_2 concentration over consecutive LD intervals with increasing Ci concentrations (0 to ~ 4 mM). Light and dark intervals during the assay lasted 6 min. Simultaneous measurements of the CO_2 concentration enabled us to determine the CO_2 uptake and HCO_3^- uptake kinetics according to equations by Badger et al. (1994), using a photosynthetic quotient (PQ) of 1.4 (Williams and Robertson, 1991). All measurements were performed in f/2 medium with ca. 300 µM NO_3^- for high NO_3^--grown cells and ca. 10 µM NO_3^- for low NO_3^--grown cells and buffered with 50 mM HEPES (pH 8.0) at 15°C. Dextran-bound sulfonamide (DBS), a membrane-impermeable inhibitor of external carbonic anhydrase (CA), was added to the cuvette to a final concentration of 100 µM. Chl *a* concentration ranged between 0.5 and 1 mg mL^{-1}. The incident photon flux density was 300 µmol photons m^{-2} s^{-1}. For further details on the method and calculation, we refer to Badger et al. (1994) and Rost et al. (2007). The kinetic parameters V_{max} and $K_{1/2}$ were calculated from the Michaelis Menten equation.

Furthermore, net photosynthesis was measured under various light intensities (0 to 800 µmol photons m^{-2} s^{-1}). While the same buffer (HEPES 50 mM, pH 8.0) and respective NO_3^- concentrations (300 versus 10 µM) were used as in the Ci flux assay measurements, the Ci

concentration were kept at ~ 2 mM. This way rates of photosynthesis, both expressed in terms of O_2 evolution and C fixation, could be measured as a function of PFD. The rate of photosynthesis (light-saturated photosynthetic rate) P was calculated from the equation

$P = \mathrm{Pm}(1 - \exp(-P1(x - P2)))$. The apparent Chl α specific efficiency of light harvesting α was calculated from the equation $\alpha = Pm * P1$, with units of µmol O_2 (mg Chl α)$^{-1}$ h^{-1} (µmol photon m^{-2} s^{-1})$^{-1}$.

2.14. Statistical analysis

All data was statistically analyzed using the T-test with a confidence level of 95%.

3. Results

3.1. Culture conditions

The cell densities of ca. 3 * 10^5 cells mL^{-1} were found to reduce TA and DIC by 20% in the high and 10% in the low NO_3^- treatment, respectively (Tab. III). Cells at a density of 3 * 10^4 and 10^5 cells mL^{-1} had no almost no impact on TA and DIC in the growth medium (Tab. III). This drift in DIC over the course of the experiment was generally low, ensuring only small changes in pH and pCO_2 and therefore is reported as a negligible effect on C and N assimilation in cells in our study.

Table III. Carbonate chemistry in the culture medium of the high (H) and low (L) NO_3^- treatments.

TA: total alkalinity; DIC: dissolved inorganic carbon; pCO_2: CO_2 partial pressure

NO_3^- treatment	Cell density (cells mL^{-1})	TA (µeq kg^{-1})	DIC (µmol kg^{-1})	pCO_2 (µatm)
H	30000	2277 ± 26	2047 ± 15	400.9
L	30000	2318 ± 21	2095 ± 6	431.5
H	100000	2242 ± 39	2024 ± 8	418.5
L	100000	2330 ± 50	2108 ± 39	438.2
H	300000	1917	1792 ± 5	~ 600
L	300000	2095	1914 ± 17	~ 500

3.2. Growth parameters

Although the growth rates were quite similar (1.1 to 1.2 d^{-1}) between high and low NO_3^--grown cells (Tab. IV), low NO_3^--grown cells accumulated less organic C and N. The cellular POC content was approximately one-third lower under low NO_3^- with values of 9.3 ± 0.8 pg $cell^{-1}$ in low and 13.9 ± 2.4 pg $cell^{-1}$ in high NO_3^--grown cells (Tab. IV; T-test: t = -3.27, p = 0.03). Similarly, low NO_3^--grown cells contained less PON (1.3 ± 0.1 pg N $cell^{-1}$) than their high NO_3^- cells counterparts (1.9 ± 0.2 pg N $cell^{-1}$) (Tab. IV; T-test: t = -6.206, p = 0.0001). Furthermore, cells in the low NO_3^- treatment were characterized by decreased protein content as well as cell size. The cellular protein content was about one-third lower when cells were cultured under low NO_3^- with values up to 1.2 ± 0.1 pg $cell^{-1}$ compared to a protein content of 1.7 ± 0.1 pg $cell^{-1}$ under high NO_3^- (Tab. IV; T-test: t = -10.606, p = 0.0004). The cell volume under low NO_3^- was ca. one-fourth lower (272 ± 37 μm^3) compared to high NO_3^- (394 ± 46 μm^3) (Tab. IV; T-test: t = -4.606, p = 0.001). Despite changes in POC and PON, the C to N ratio remained constant and was about 8.3 to 8.5 in both NO_3^- treatments (Tab. IV). POC production was significantly higher under high NO_3^- in comparison with low NO_3^-–grown cells, being 16.7 ± 2.8 pg C $cell^{-1}$ d^{-1} and 10.4 ± 1.2 pg C $cell^{-1}$ d^{-1}, respectively (Fig. 9A, T-test: t = 3.578, p = 0.023). The PON production under high NO_3^- was 2.3 ± 0.3 pg N $cell^{-1}$ d^{-1} whereas under low NO_3^- was 1.4 ± 0.2 pg N $cell^{-1}$ d^{-1} (Fig. 9B, T-test: t = -7.361, p = 0.00002).

The cellular PIC content also decreased with decreasing NO_3^- availability. Low NO_3^--grown cells contained 6.6 ± 0.9 pg C $cell^{-1}$ whereas high NO_3^--grown cells had a PIC content of 8.7 ± 0.9 pg C $cell^{-1}$ (Tab. IV, T-test: t = -2.763, p = 0.05). The PIC to POC ratio was 0.6 to 0.7 (as can be calculated from the POC and PIC values in Tab. IV) and remained constant irrespective of the tested NO_3^- levels. PIC production was 10.5 ± 1.1 pg C $cell^{-1}$ d^{-1} under high NO_3^- and 7.3 ± 1 pg C $cell^{-1}$ d^{-1} under low NO_3^- (Fig. 9C, T-test: t = -3.64, p = 0.021).

Cells grown under low NO_3^- produced 0.2 ± 0.2 % normal coccoliths, 88.3 ± 0.5 % incomplete coccoliths, 0 % malformed coccoliths, and 11.5 ± 0.5 % incomplete and malformed coccoliths (Fig. 10 and 11). Cells grown under high NO_3^- produced 96.2 ± 1.9 % normal coccoliths, 2.4 ± 1.4 % incomplete coccoliths, 1.3 ± 0.5 % malformed coccoliths, and 0.1 ± 0.2 % incomplete and malformed coccoliths (Fig. 10 and 11). The number of visible coccoliths per cell was 6.3 ± 0.1 under high and 6.9 ± 0.4 under low NO_3^-.

Table IV. Growth rate (μ), cell volume (CV), particulate organic carbon (POC), particulate inorganic carbon (PIC), particulate organic nitrogen (PON), protein content and C to N ratio in cells grown under high (H) and low (L) NO_3^-.

The values represent the means of triplicate incubations (± SD).

NO_3^- treatment	μ (d^{-1})	CV (μm^3)	POC (pg $cell^{-1}$)	PIC (pg $cell^{-1}$)	PON (pg $cell^{-1}$)	Protein (pg $cell^{-1}$)	C to N ratio
H	1.2 ± 0.1	394 ± 46	13.9 ± 2.4	8.7 ± 0.9	1.9 ± 0.2	1.7 ± 0.1	8.5 ± 0.5
L	1.1 ± 0.2	272 ± 37	9.3 ± 0.8	6.6 ± 0.9	1.3 ± 0.1	1.2 ± 0.1	8.3 ± 0.9

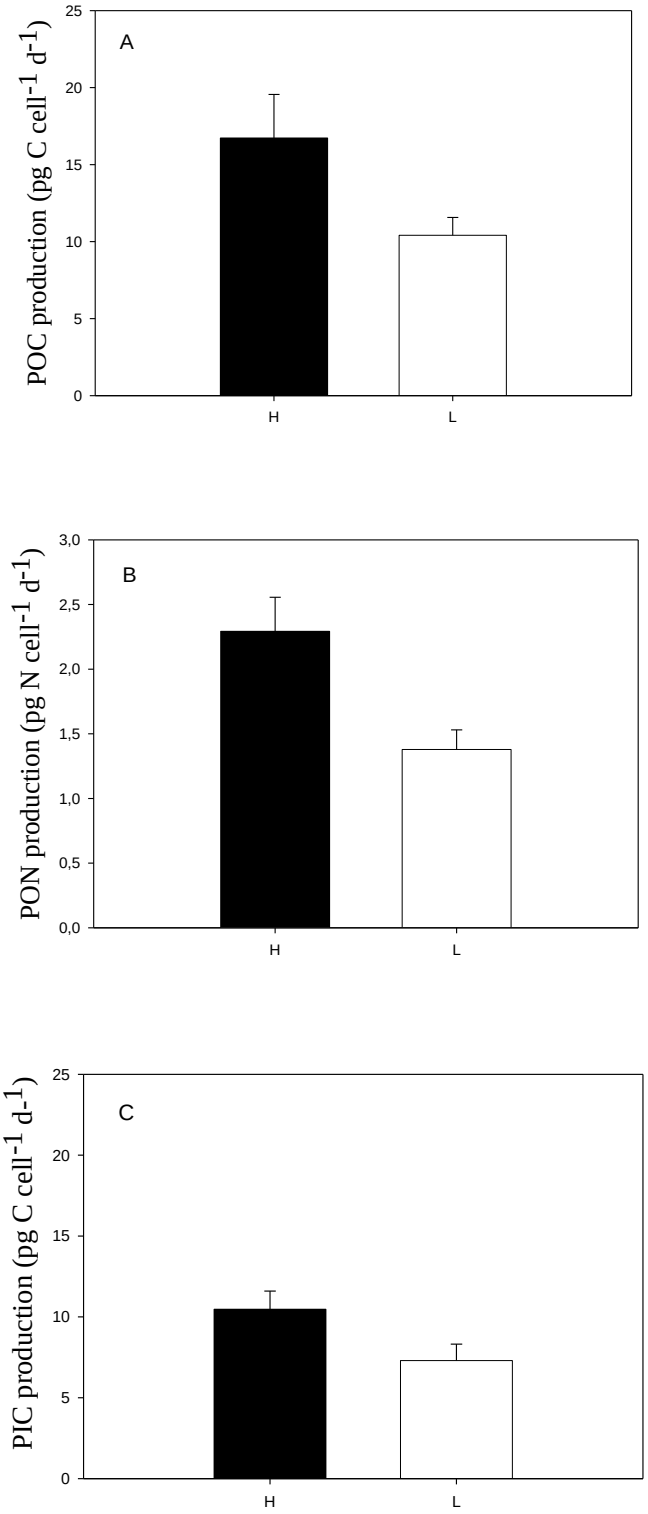

Figure 9. Effects of high (■) and low (□) NO_3^- on particulate organic carbon (POC) production (A), particulate organic nitrogen (PON) production (B) and particulate inorganic carbon (PIC) production (C) in *E. huxleyi* cells. Values represent the means of triplicate incubations (± SD).

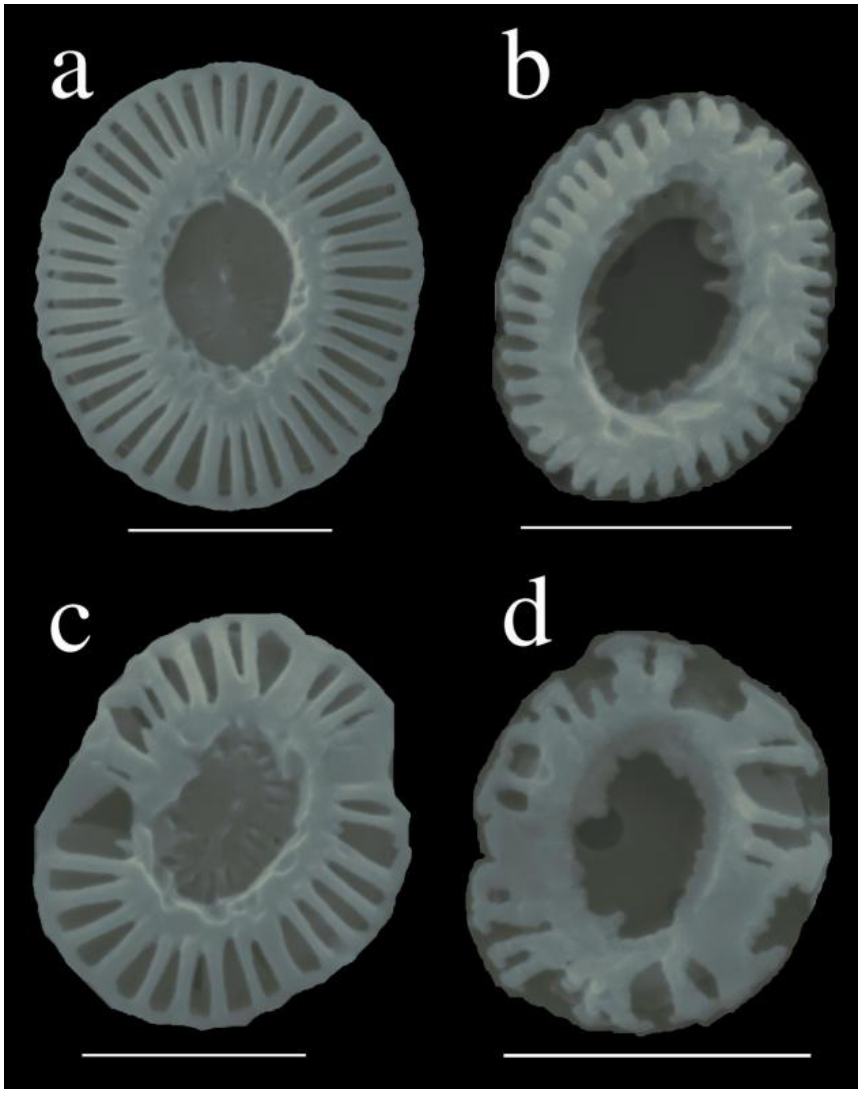

Figure 10. Scanning electron microscopy images of coccoliths of *E. huxleyi*. All scalebars 2 µm. All specimens in distal view. (a) normal coccolith. (b) incomplete coccolith. (c) malformed coccolith. (d) incomplete and malformed coccolith.

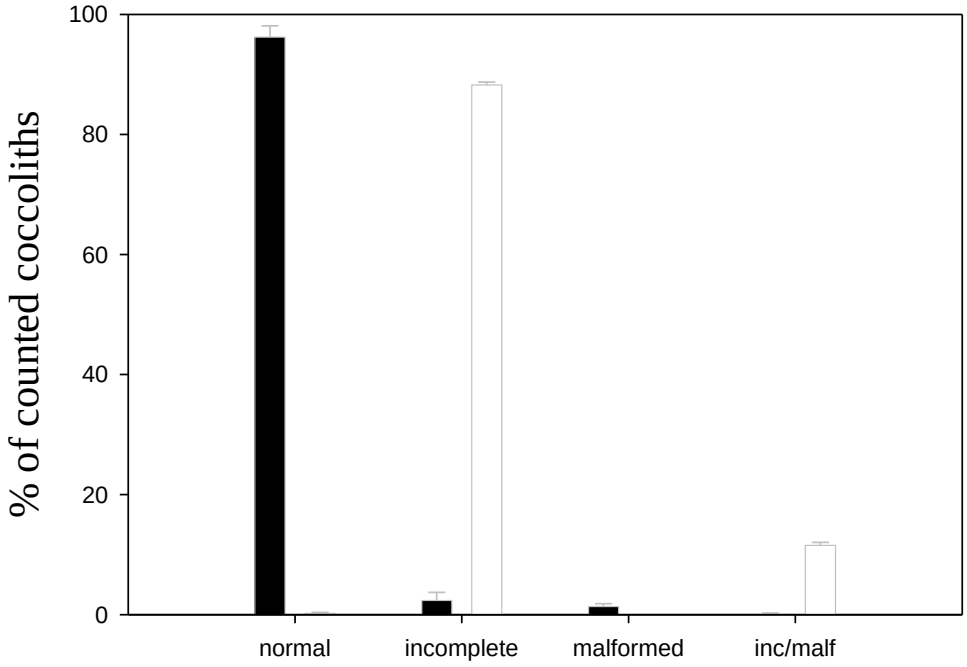

Figure 11. Percentage of normal, malformed, incomplete, and incomplete and malformed (inc/malf) coccoliths under high (■) and low (□) NO_3^-. Values represent an average of duplicates (±SD).

3.3. Macromolecular composition

Nitrate availability caused an allocation of macromolecular pools in cells in our study. While the protein to lipid ratio decreased under low NO_3^-, the ratios of proteins to carbohydrates and lipids to carbohydrates increased. The protein to lipid ratio was 11.6 ± 2.2 under low NO_3^- compared to a value of 15.4 ± 1.2 under high NO_3^- (Fig. 12A). The ratio of proteins to carbohydrates was 3 ± 0.3 (10^{-4}) in low NO_3^- -grown cells and 2.1 ± 0.3 (10^{-4}) in high NO_3^- -grown cells (Fig. 12B). Similarly, the ratio of lipids to carbohydrates was 2.7 ± 0.6 (10^{-6}) under low NO_3^-and1.4 ± 0.1 (10^{-6}) in cells under high NO_3^- (Fig. 12C).

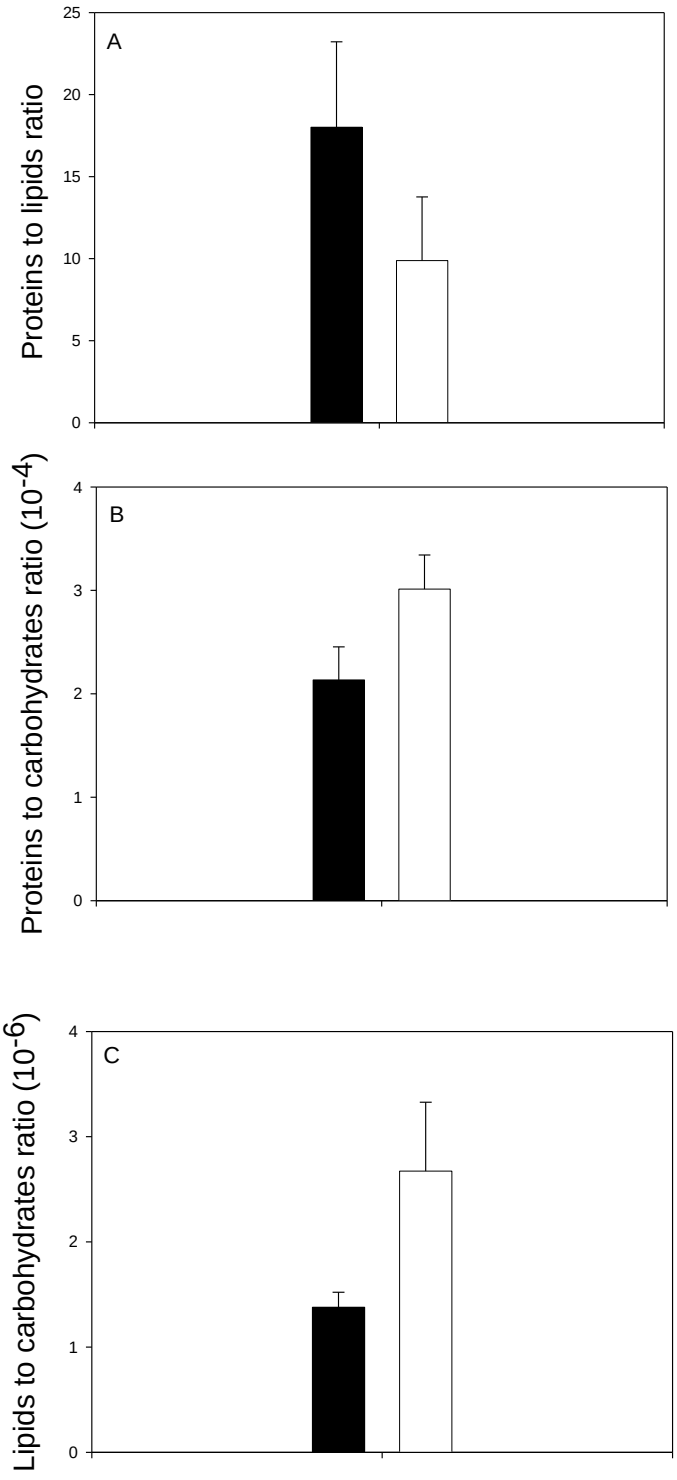

Figure 12. The ratios of proteins to lipids (A), proteins to carbohydrates (B) and lipids to carbohydrates (C) in cells under high (■) and low (□) NO_3^-. Values represent an average of triplicates (±SD).

3.4. Nitrate assimilation

Nitrate availability was found to affect the kinetics of both NR and NiR. NR V_{max} was 1.7-fold lower in cells under low NO_3^- (0.64 ± 0.06 fmol NO_2^- min^{-1} $cell^{-1}$) compared to high NO_3^--grown cells (1.09 ± 0.25 fmol NO_2^- min^{-1} $cell^{-1}$), when it was expressed on a cell basis (Tab. V; T-test: t = -3.037, p = 0.038). When expressed on a protein basis, cell volume, C or N, NR V_{max} was unaffected by the NO_3^- concentration in the medium. The Michaelis-Menten constant (K_m) of NR for NO_3^- differed between high and low NO_3^--grown cells and was significantly lower in low NO_3^- cells. Cells at high NO_3^- had a K_m of NR for NO_3^- of 0.099 ± 0.013 mM, whereas under low NO_3^- the K_m of NR for NO_3^- was 0.074 ± 0.007 mM (Tab. V; T-test: t = -2.952, p = 0.041; Fig. 13A). The K_m of NR for NADH was not significantly different between high and low NO_3^--grown cells (Tab. IV; Fig. 13B). Regardless of the basis on which it was expressed, NiR V_{max} was lower under low NO_3^- availability in the growth

Table V. Kinetics V_{max} and K_m of NR and NiR in cells grown under high (H) and low (L) NO_3^-.

All values represent the means of triplicates (± SD).

NO_3^- treatment			H	L
NR	V_{max}	fmol NO_2^- min^{-1} $cell^{-1}$	1.09 ± 0.25	0.64 ± 0.06
	K_m (NO_3^-)	mmol L^{-1}	0.099 ± 0.013	0.074 ± 0.007
	K_m (NADH)	mmol L^{-1}	0.25 ± 0.013	0.206 ± 0.025
NiR	V_{max}	fmol NO_2^- min^{-1} $cell^{-1}$	0.56 ± 0.05	0.3 ± 0.01
	K_m (NO_2^-)	mmol L^{-1}	3.14 ± 0.6	1.69 ± 0.43

medium (Tab. V). NiR V_{max} was 0.3 ± 0.01 fmol NO_2^- min^{-1} $cell^{-1}$ in cells grown under low NO_3^- and 1.9-fold higher (0.56 ± 0.05 fmol NO_2^- min^{-1} $cell^{-1}$) in cells grown under high NO_3^- (Tab. V; T-test: t=-9.212, p=0.0007). Also, the K_m of NiR for NO_2^- was substantially lower under low NO_3^- (1.69 ± 0.43 mM in low and 3.14 ± 0.6 mM in high NO_3^--grown cells; Tab. V; T-test: t=-3.408, p=0.027; Fig. 14).

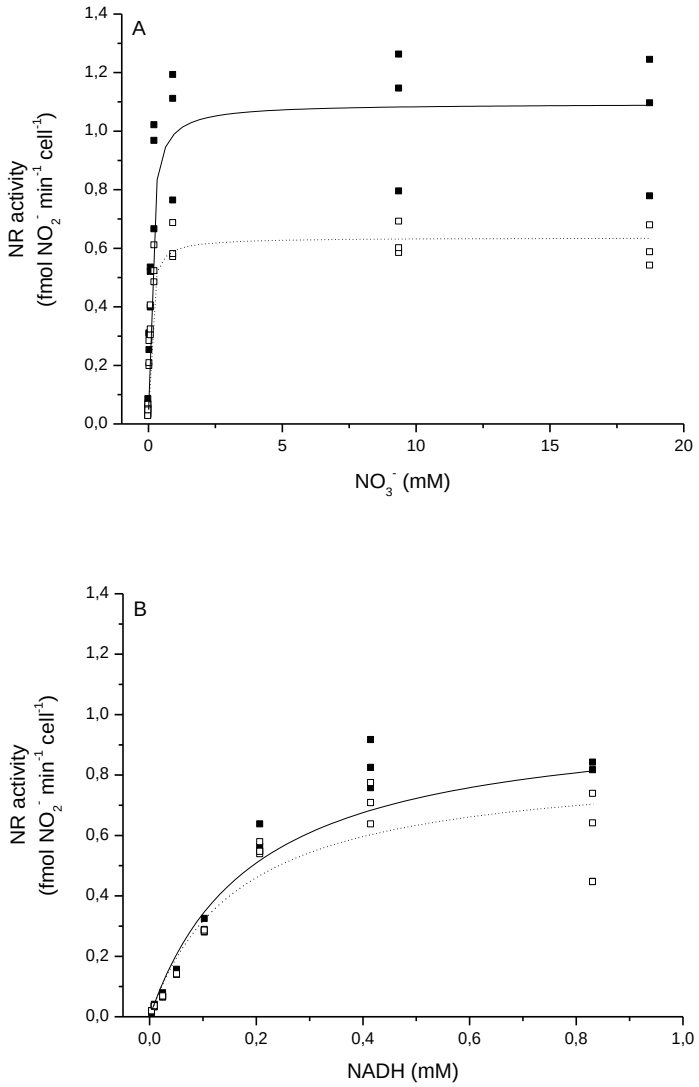

Figure 13. Kinetic curve of nitrate reductase (NR) for NO_3^- (A) and NADH (B) in cells grown under high (■) and low (□) NO_3^-. All values represent the means of triplicates.

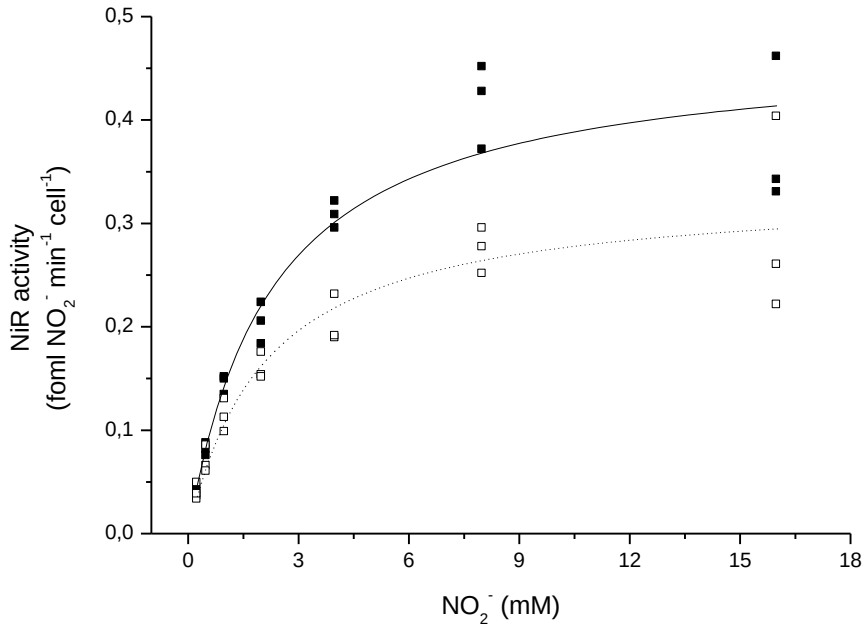

Figure 14. Kinetic curve of nitrite reductase (NiR) for NO_2^- in cells grown under high (■) and low (□) NO_3^-. All values represent the means of triplicates.

The different NO_3^- concentrations also affected GS kinetics. GS V_{max} in low NO_3^--grown cells was about one-fourth higher than under high NO_3^- (Tab. VI; T-test: t=-3.529, p=0.01). GS V_{max} was higher in low NO_3^--grown cells and this relationship was independent of the type of normalization (protein, cell volume, cell C or N). The K_m for glutamate was two-fold lower in low NO_3^--grown cells (1.612 ± 0.37 mM) than in their counterparts (3.812 ± 1.63 mM) (Tab. VI; T-test: t=-3.529, p=0.01; Fig. 15). The K_m for ATP and NH_2OH were similar between high and low NO_3^--grown cells (Tab. VI; Fig. 16A and 16B). GOGAT V_{max} was 3.91 ± 0.76 fmol NADH min^{-1} $cell^{-1}$ under low NO_3^- and 2.87 ± 0.18 fmol NADH min^{-1} $cell^{-1}$ under high NO_3^-, showing a significant difference in its activity between the two NO_3^- regimes (Tab. VI; T-test: t = 2.639, p = 0.025). When activities were expressed on protein, cell volume, C or N basis, GOGAT V_{max} was also higher in low NO_3^--grown cells. The V_{max} of the anaplerotic

enzyme PEPCK was about 1.6-fold lower in low NO_3^- grown-cells compared to high NO_3^--grown cells, with values of 4.66 ± 0.45 fmol NADH min^{-1} $cell^{-1}$ under low and 7.29 ± 0.28 fmol NADH min^{-1} $cell^{-1}$ under high NO_3^- (Tab. VI; T-test: t = -5.697, p = 0.001). When normalized on protein, cell volume, C or N, however, PEPCK V_{max} did not differ between high and low NO_3^- cells.

Table VI. Kinetics V_{max} and K_m of GS, as well as the activities (V_{max}) of GOGAT and PEPCK in cells grown under high (H) and low (L) NO_3^-.

All values represent the means of triplicates (± SD). One unit is equal to 1 fmol L-Glu γ-monohydroxamate.

NO_3^- treatment			H	L
GS	V_{max}	units min^{-1} $cell^{-1}$	0.385 ± 0.11	0.57 ± 0.04
	K_m (ATP)	mmol L^{-1}	0.513 ± 0.157	0.344 ± 0.05
	K_m (NH_2OH) (n=4)	mmol L^{-1}	0.095 ± 0.035	0.092 ± 0.023
	K_m (Glu)	mmol L^{-1}	3.812 ± 1.63	1.621 ± 0.372
GOGAT	V_{max}	fmol NADH min^{-1} $cell^{-1}$	2.87 ± 0.18	3.91 ± 0.76
PEPCK	V_{max}	fmol NADH min^{-1} $cell^{-1}$	7.29 ± 0.28	4.66 ± 0.45

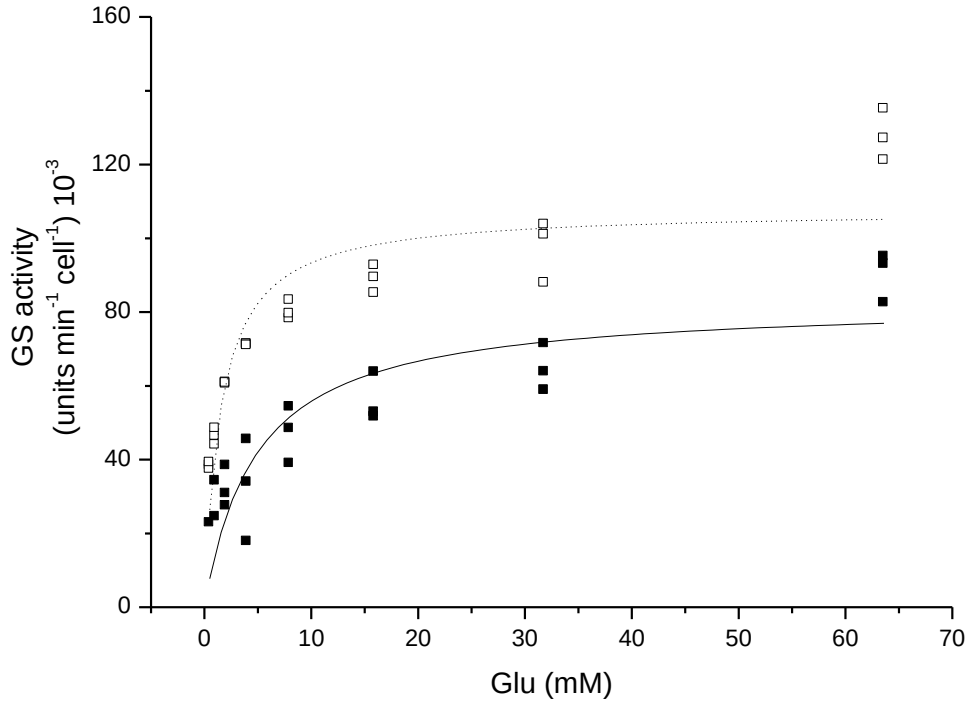

Figure 15. Kinetic curve of GS for glutamate (Glu) in cells grown under high (■) and low (□) NO_3^-. One unit is equal to 1 fmol L-Glu γ-monohydroxamate. All values represent the means of triplicates.

3.5. Glutamine synthetase isoforms

After separation on the Sephacryl S-200 HR column, two fractions showed GS activity and were recognized as the chloroplastic (GS_2) and cytosolic (GS_1) isoform, according to their retention times (51-54 min for GS_2 and 62-65 min for GS_1, respectively, Fig. 17A and 17B).

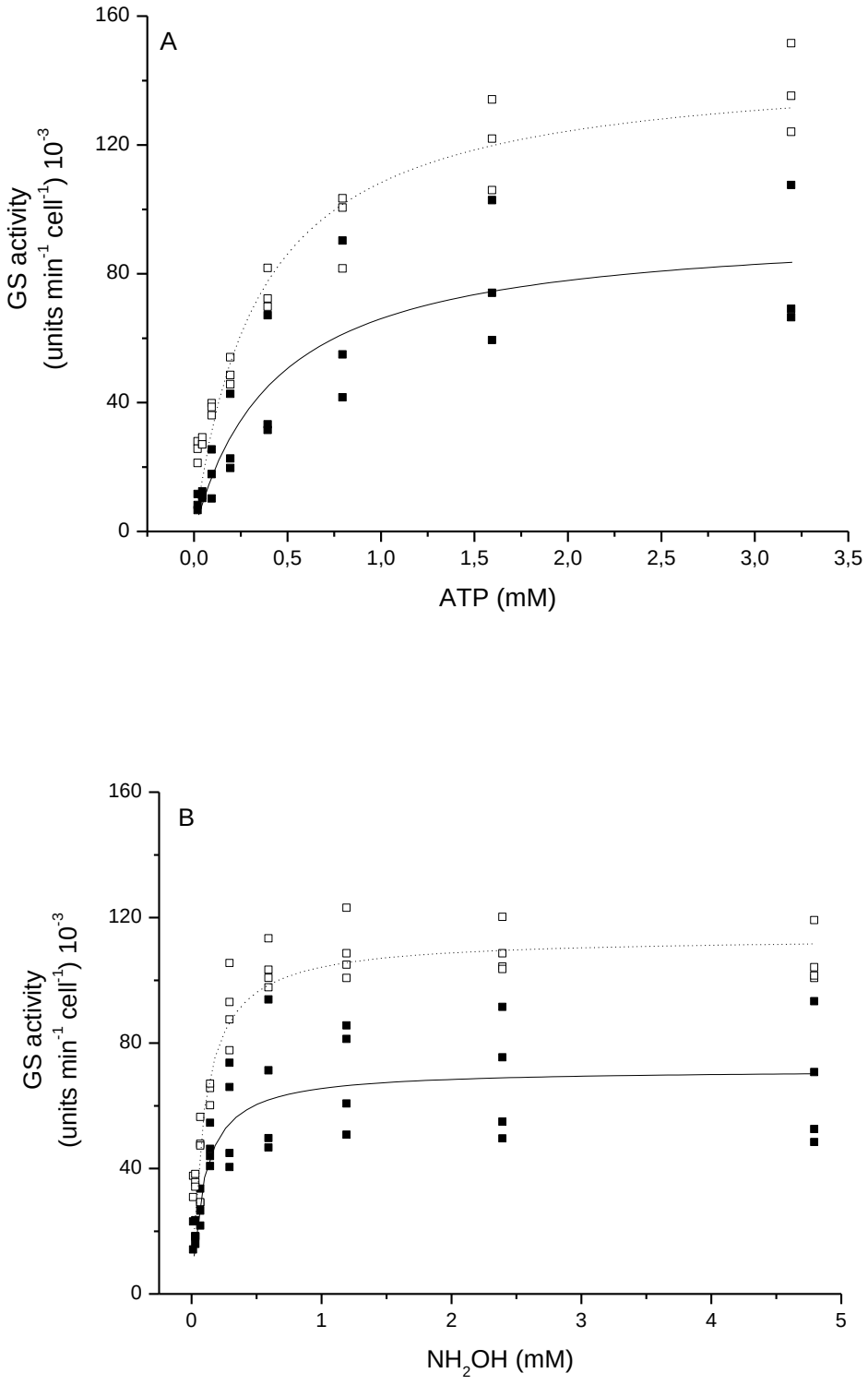

Figure 16. Kinetic curve of GS for ATP (A) and NH_2OH (B) in cells grown under high (■) and low (□) NO_3^-. One unit is equal to 1 fmol L-Glu γ-monohydroxamate. In the kinetics of GS for ATP (n=3) and for NH_2OH (n=4).

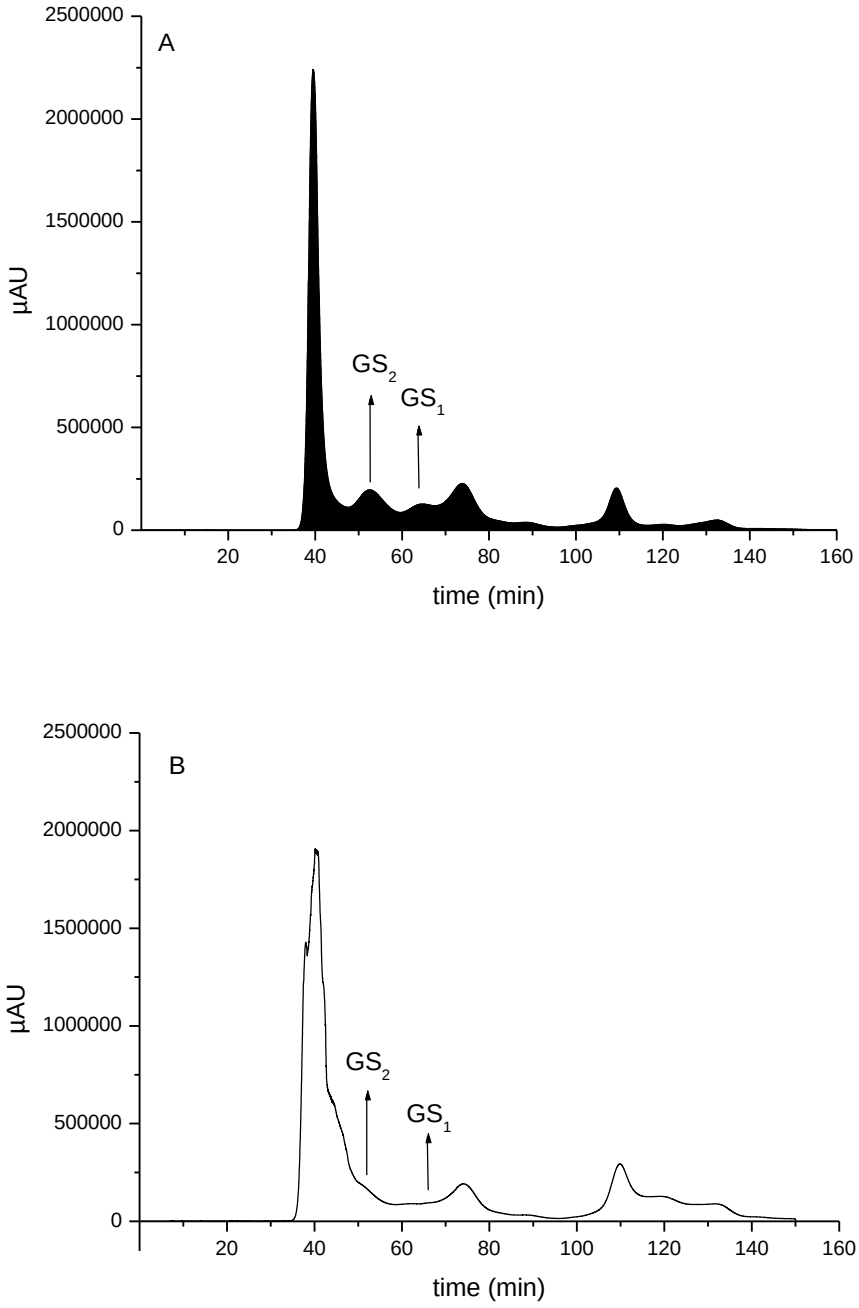

Figure 17. Purification of the GS isoforms in cells grown under high (■) (A) and low (□) (B) NO_3^- using a Sephacryl S-200 HR column. GS active fractions are shown with arrows.

Under high NO_3^-, the relative and specific activities of GS_1 were higher than GS_2 activity (Fig. 18A and 18B). On the opposite, both relative and specific activities of GS_2 were higher than GS_1 activity under low NO_3^- (Fig. 18A and 18B). After application on the HiTrap Blue

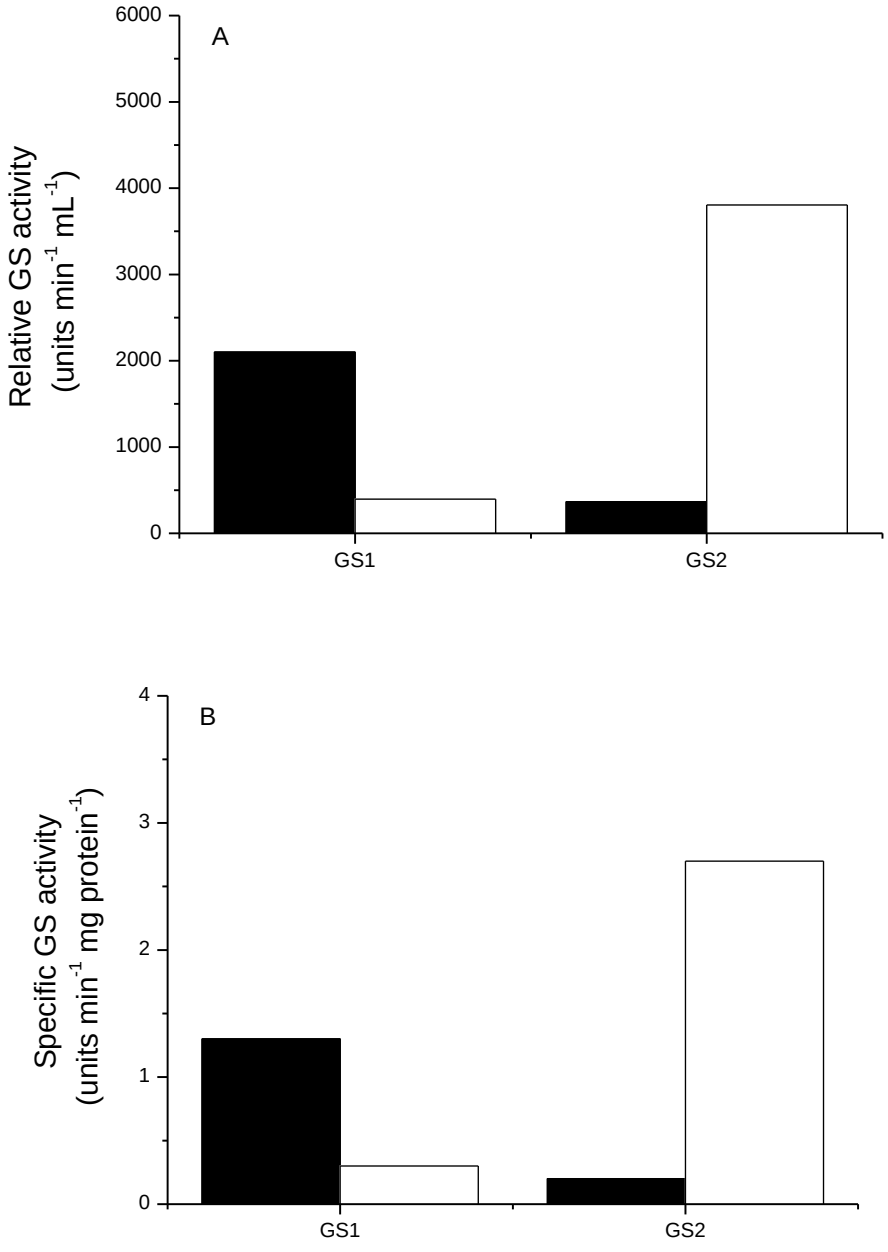

Figure 18. Relative (A) and specific (B) activities (x5) of the GS_1 and GS_2 isoforms in high (■)and low (□) NO_3^--grown cells after separation on the Sephacryl S-200 HR column. GS_1: cytosolic isoform; GS_2: chloroplastic isoform.

HP column, GS_1 was eluted after 1-2 min and GS_2 after 7-8 min in both NO_3^- treatments (data not shown). After application of the GS active fractions on the MonoQ column, GS_1 was eluted after 4 min and GS_2 after 15-16 min in both NO_3^- treatments (Fig. 19A, 19B, 20A and 20B). GS_1 in low NO_3^- -grown cells could not be further purified on the MonoQ column.

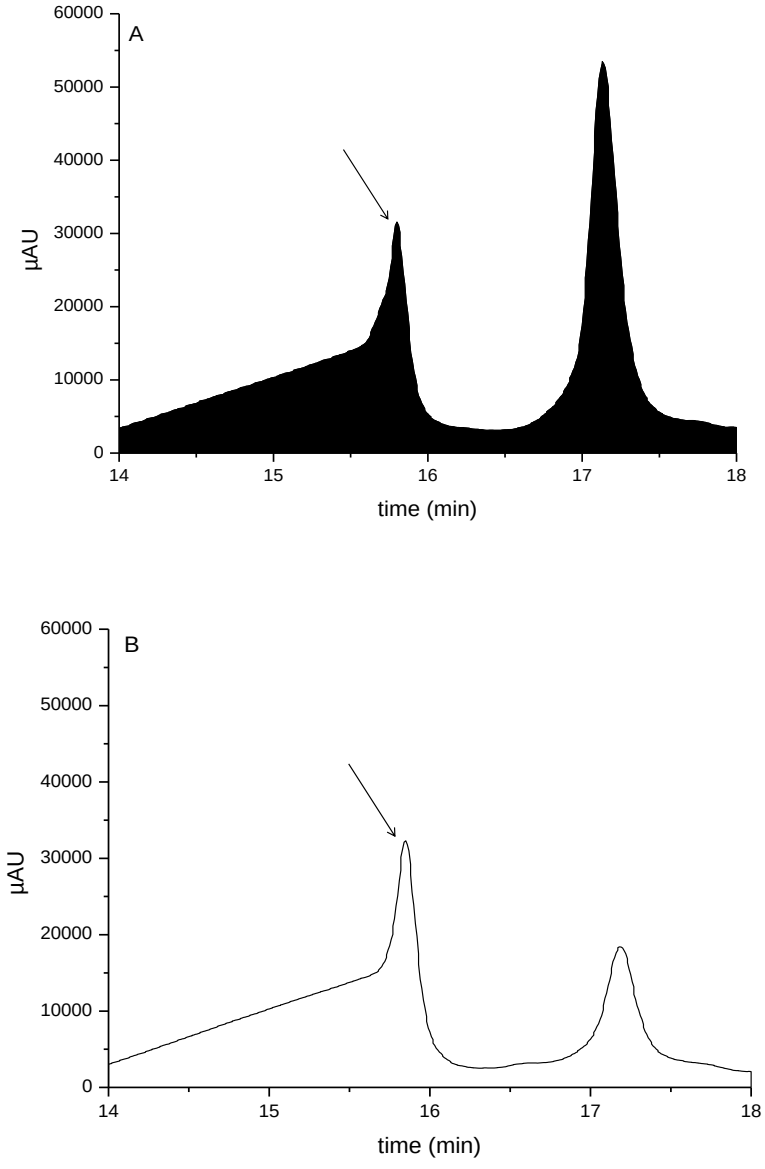

Figure 19. Purification of the GS_2 isoform in cells grown under high (■) (A) and low (□) (B) NO_3^- using a MonoQ column. GS active fractions are shown with arrows.

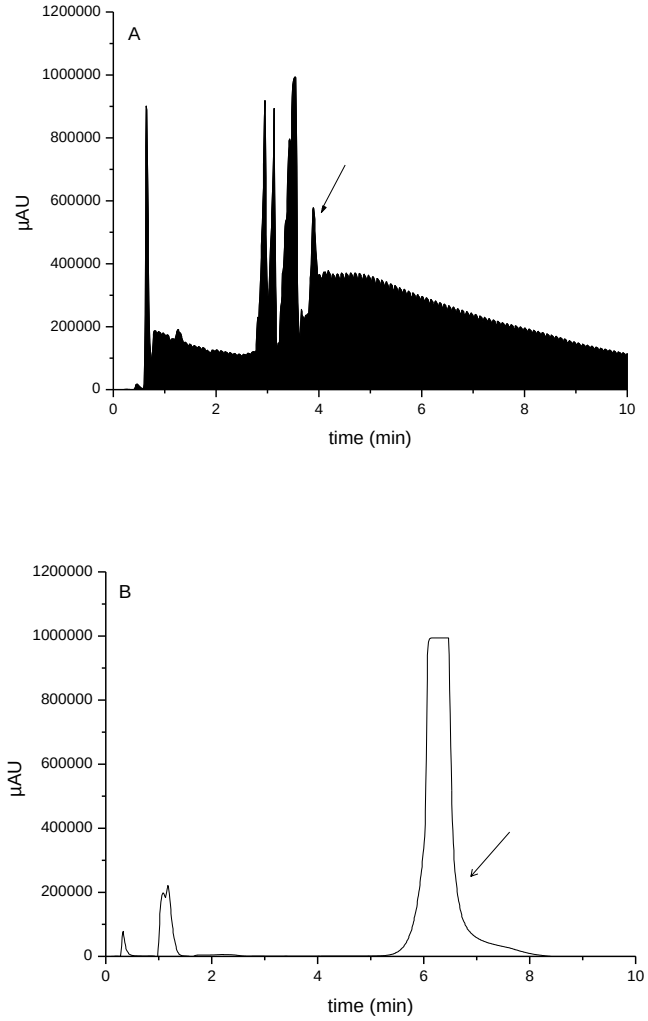

Figure 20. Purification of the GS_1 isoform in cells grown under high (■) (A) and low (□) (B) NO_3^- using a MonoQ column. GS active fractions are shown with arrows. The GS_1 isoform could not be further purified in the MonoQ column under low NO_3^-.

The relative GS_1 and GS_2 activities from the fractions of the HiTrap Blue HP and MonoQ column are shown in Tab. VII. An aliquot of the GS active fraction of high and low NO_3^- -grown cells (after the MonoQ 5/50 GL column) was applied on a 10% SDS-PAGE gel and a protein band at ca. 45 kDa was detected (Fig. 21). Due to the low protein amount of the

Table VII. Purification of GS isoforms in *E. huxleyi* cells grown under high (H) and low (L) NO_3^- (GS_1: cytosolic GS isoform; GS_2: chloroplastic GS isoform).

GS activity was measured according to the GS synthetase assay. Relative GS activity is given in nmol L-Glu γ-monohydroxamate min^{-1} mL^{-1}. Specific GS activity is given in nmol L-Glu γ-monohydroxamate min^{-1} mg $protein^{-1}$.

NO_3^- treatment	Purification step	GS isoforms	Relative GS activity	Specific GS activity	Purification factor
H		Crude extract	951	0.3	1
	Sephacryl S-200 HR	GS_1	2100	1.3	4.3
		GS_2	395	0.3	1
	HiTrap Blue HP	GS_1	913	3	10
		GS_2	213	-	-
	MonoQ 5/50 GL	GS_1	89	102	340
		GS_2	24	-	-
L		Crude extract	1918	0.55	1
	Sephacryl S-200 HR	GS_1	365.5	0.2	-
		GS_2	3805	2.7	4.9
	HiTrap Blue HP	GS_1	304.5	-	-
		GS_2	2039.5	6.8	12.3
	MonoQ 5/50 GL	GS_1	6	-	-
		GS_2	113	-	-

purified GS isoforms, only the GS_1 isoform of high NO_3^- -grown cells was clearly visualized after silver staining. This gives some evidence that GS_1 protein expression is increased under high NO_3^-.

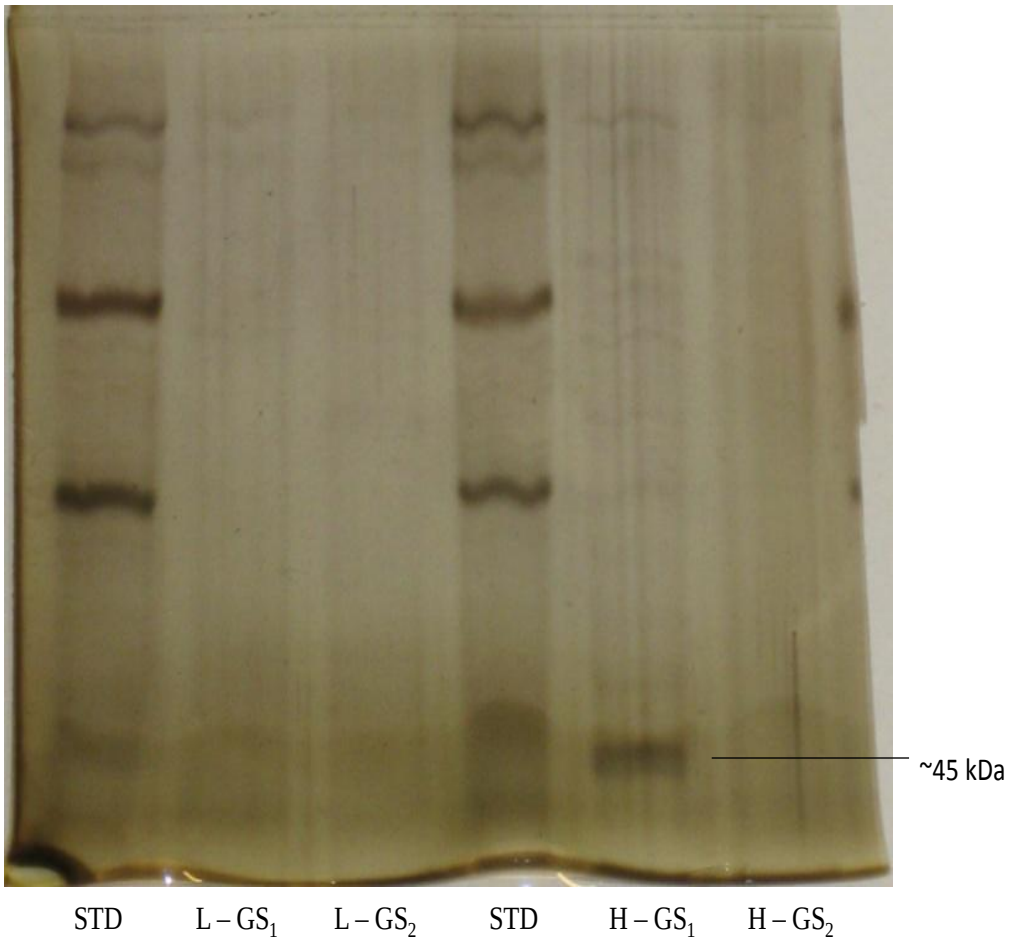

Figure 21. An aliquot of the glutamine synthetase (GS) active fractions after separation on a MonoQ 5/50 GL column was applied on a 10 % SDS-PAGE gel. A band at approximately 45 kDa was visualized after silver staining (Std: protein standard – ovalalbumin: 45 kDa).

3.6. Photosynthesis and respiration

The maximum rate of net photosynthesis (V_{max}) expressed on a per cell basis was about two-fold lower in low NO_3^--grown cells, with a value of 6.5 ± 0.8 fmol O_2 min^{-1} $cell^{-1}$ compared to 12.9 ± 0.7 fmol O_2 min^{-1} $cell^{-1}$ under high NO_3^- (Tab. VIII; t = -3.063, p = 0.022; Fig. 22). When net photosynthesis was expressed on a per mg chl α basis, no difference of its rate was observed between high and low NO_3^--grown cells. The amount of Chl *α* was about two-fold lower in cells under low NO_3^- (data not shown). However, the $K_{1/2}$ of photosynthesis for CO_2 and DIC was lower in low NO_3^--grown cells (Fig. 22A and 22B). The $K_{1/2}$ (CO_2) of photosynthesis was 4.1 ± 0.6 µM in high and 2.5 ± 0.6 µM in low NO_3^--grown cells (Tab. VIII; t = -3.158, p = 0.019), and the $K_{1/2}$ (DIC) was 443 ± 79 µM in high and 263 ± 57 µM in low NO_3^--grown cells (Tab. VIII; t = -2.639, p = 0.038). The light curve of net photosynthesis revealed that the α value was similar between the two NO_3^- treatments (1.47 ± 0.21 for high and 1.39 ± 0.06 for low NO_3^--grown cells; Tab. VIII; Fig. 23). The rate of respiration expressed on a per cell basis was similar between high and low NO_3^--grown cells (ca. 2 fmol O_2 min^{-1} $cell^{-1}$) (Tab. VIII; t = -1.59, p = 0.163). When respiration was expressed on mg Chl *α* basis, its rate was higher under low NO_3^-.

Table VIII. Kinetics V_{max} and $K_{1/2}$ of net photosynthesis, apparent Chl α specific efficiency of light harvesting (α), kinetics of gross CO_2 uptake, net CO_2 uptake and HCO_3^- uptake, as well as respiration in cells grown under high (H) and low (L) NO_3^-.

For net photosynthesis, gross and net CO_2 uptake, HCO_3^- uptake and respiration in cells grown under high (H) NO_3^- (n=5). All other values represent the means of triplicates (± SD).

NO_3^- treatment			H	L
Net photosynthesis	V_{max}	fmol O_2 min^{-1} $cell^{-1}$	12.9 ± 0.7	6.5 ± 0.8
	$K_{1/2}$ (CO_2)	µmol L^{-1}	4.1 ± 0.6	2.5 ± 0.6
	$K_{1/2}$ (DIC)	µmol L^{-1}	443 ± 79	263 ± 57
α		µmol O_2 (mg Chl *a*)$^{-1}$ h^{-1} (µmol photon m^{-2} s^{-1})$^{-1}$	1.5 ± 0.2	1.4 ± 0.1
Gross CO_2 uptake	V_{max}	fmol CO_2 min^{-1} $cell^{-1}$	6.1 ± 1.9	4.5 ± 1.2
	$K_{1/2}$ (CO_2)	µmol L^{-1}	3.5 ± 0.5	2.2 ± 0.3
Net CO_2 uptake	V_{max}	fmol CO_2 min^{-1} $cell^{-1}$	2 ± 0.4	2.8 ± 0.5
	$K_{1/2}$ (CO_2)	µmol L^{-1}	5 ± 1.6	4.4 ± 1.7
HCO_3^- uptake	V_{max}	fmol HCO_3^- min^{-1} $cell^{-1}$	8.2 ± 0.6	2.4 ± 0.3
	$K_{1/2}$ (HCO_3^-)	µmol L^{-1}	502 ± 133	192 ± 21
Respiration	V_{max}	fmol O_2 min^{-1} $cell^{-1}$	2.3 ± 0.4	1.9 ± 0.1

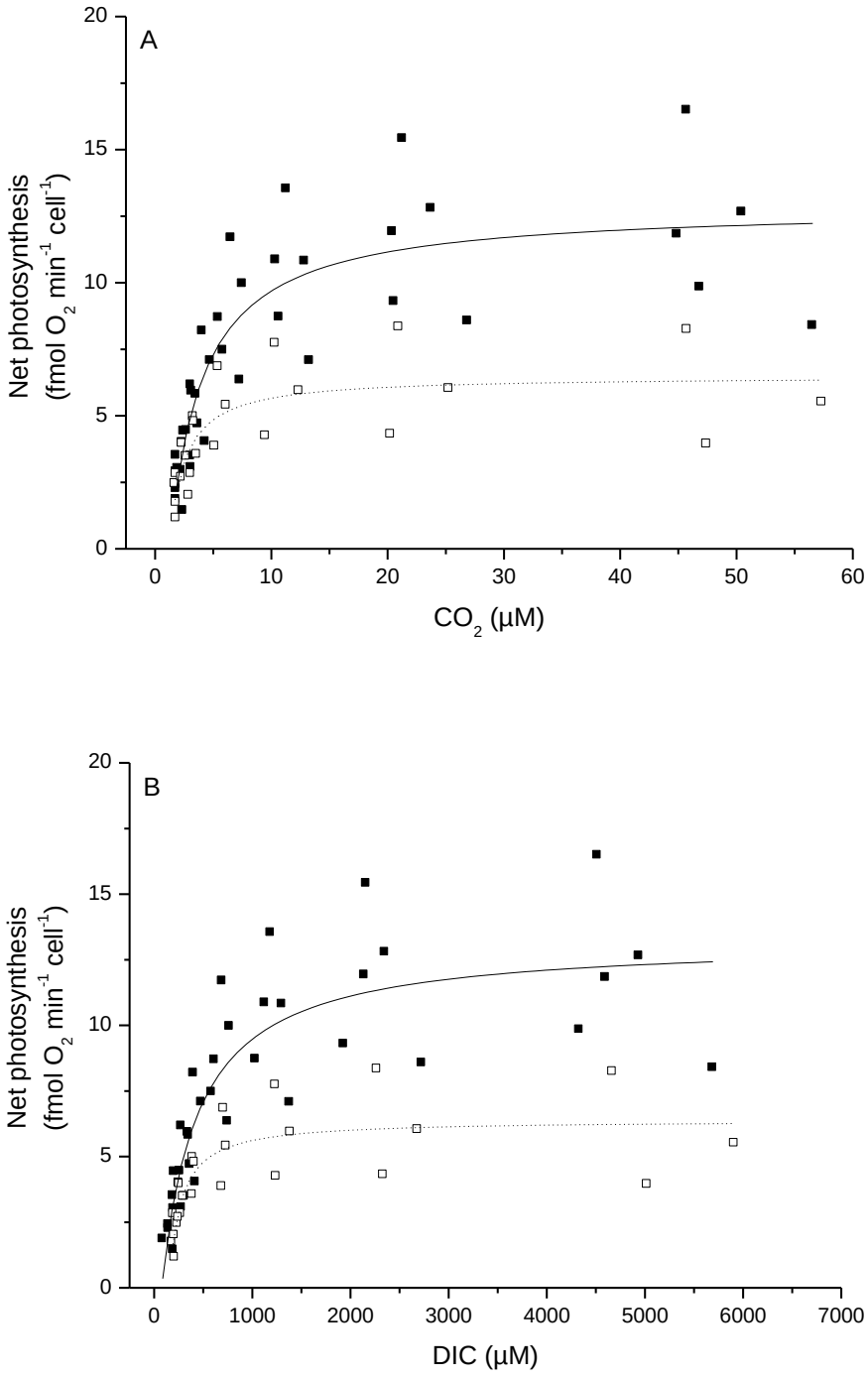

Figure 22. Kinetic curve of net photosynthesis for CO_2 (A) and DIC (B) in cells grown under high (■) and low (□) NO_3^-. For net photosynthesis in cells grown under high (H) NO_3^- (n=5). All other values represent the means of triplicates.

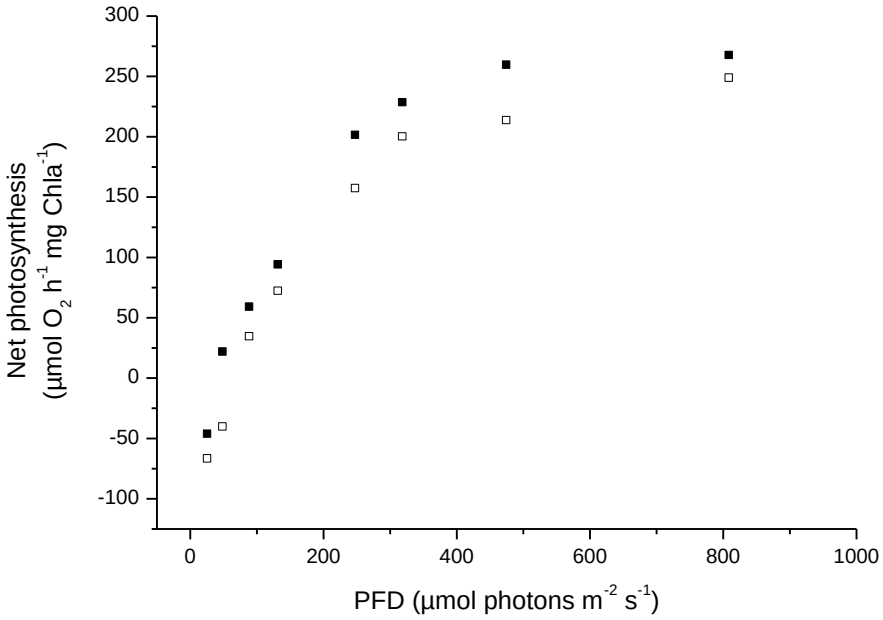

Figure 23. The effect of various light intensities (PFD) on net photosynthesis in cells grown under high (■) and low (□) NO_3^-. All values represent the means of triplicates.

3.7. Inorganic carbon fluxes

The effects of N availability were stronger on the uptake of HCO_3^- (Fig. 224). The rate of HCO_3^- uptake was approximately 4-fold lower under low NO_3^- with a value of 2.4 ± 0.3 fmol HCO_3^- min^{-1} $cell^{-1}$ compared to 8.2 ± 0.6 fmol HCO_3^- min^{-1} $cell^{-1}$ in high NO_3^--grown cells (Tab. VIII; t = -5.425, p = 0.001). While the rate of HCO_3^- uptake decreased, the affinity of HCO_3^- uptake increased under low NO_3^-. Low NO_3^--grown cells had a $K_{1/2}$ for HCO_3^- of 192 ± 21 µM compared to 502 ± 133 µM in high NO_3^--grown cells (Tab. VIII, t = -3.043, p = 0.022). Both, maximum gross and net CO_2 uptake rates (V_{max}) per cell were similar between high and low NO_3^--grown cells (Fig. 25A and 25B). The V_{max} of gross CO_2 uptake was ca. 4.5 to 6 fmol CO_2 min^{-1} $cell^{-1}$ in both high and low NO_3^--grown cells (Tab. VIII). Net CO_2 uptake V_{max} was approximately 2 to 3 fmol CO_2 min^{-1} $cell^{-1}$ in all cells (Tab. VIII). Nevertheless, low

NO_3^--grown cells had a lower $K_{1/2}$ of gross CO_2 uptake for CO_2 compared to cells under high NO_3^-. The $K_{1/2}$ of gross CO_2 uptake for CO_2 was 3.5 ± 0.5 µM under high and 2.2 ± 0.3 µM under low NO_3^- (Tab. VIII; t = -3.198, p = 0.018). The $K_{1/2}$ of net CO_2 uptake for CO_2 was about 4 to 5 µM for both high and low NO_3^--grown cells (Tab. VIII).

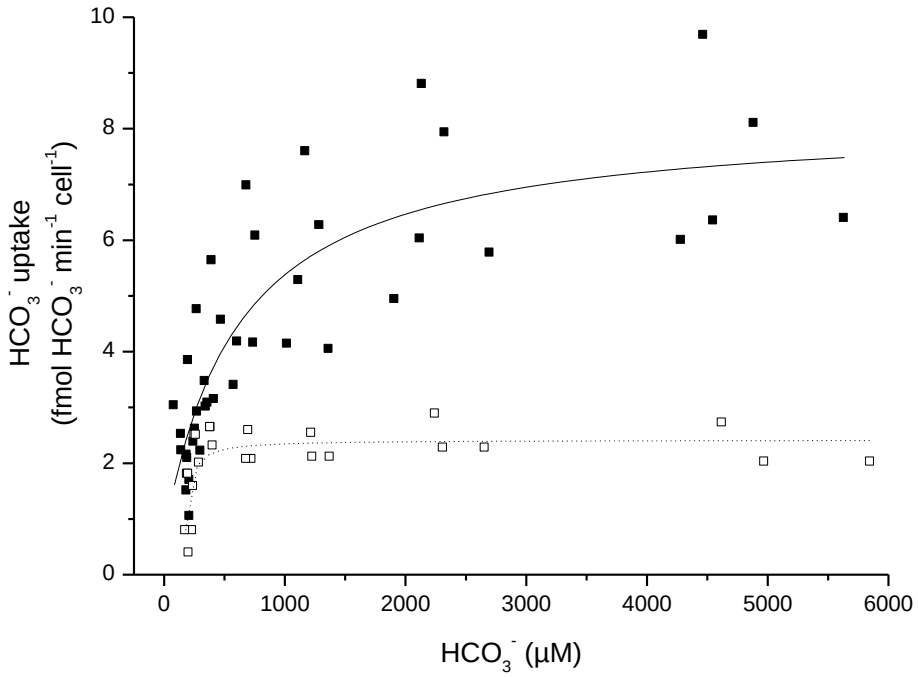

Figure 24. Kinetics of HCO_3^- uptake in cells grown under high (■) and low (□) NO_3^-. For HCO_3^- uptake in cells grown under high (H) NO_3^- (n=5). All other values represent the means of triplicates.

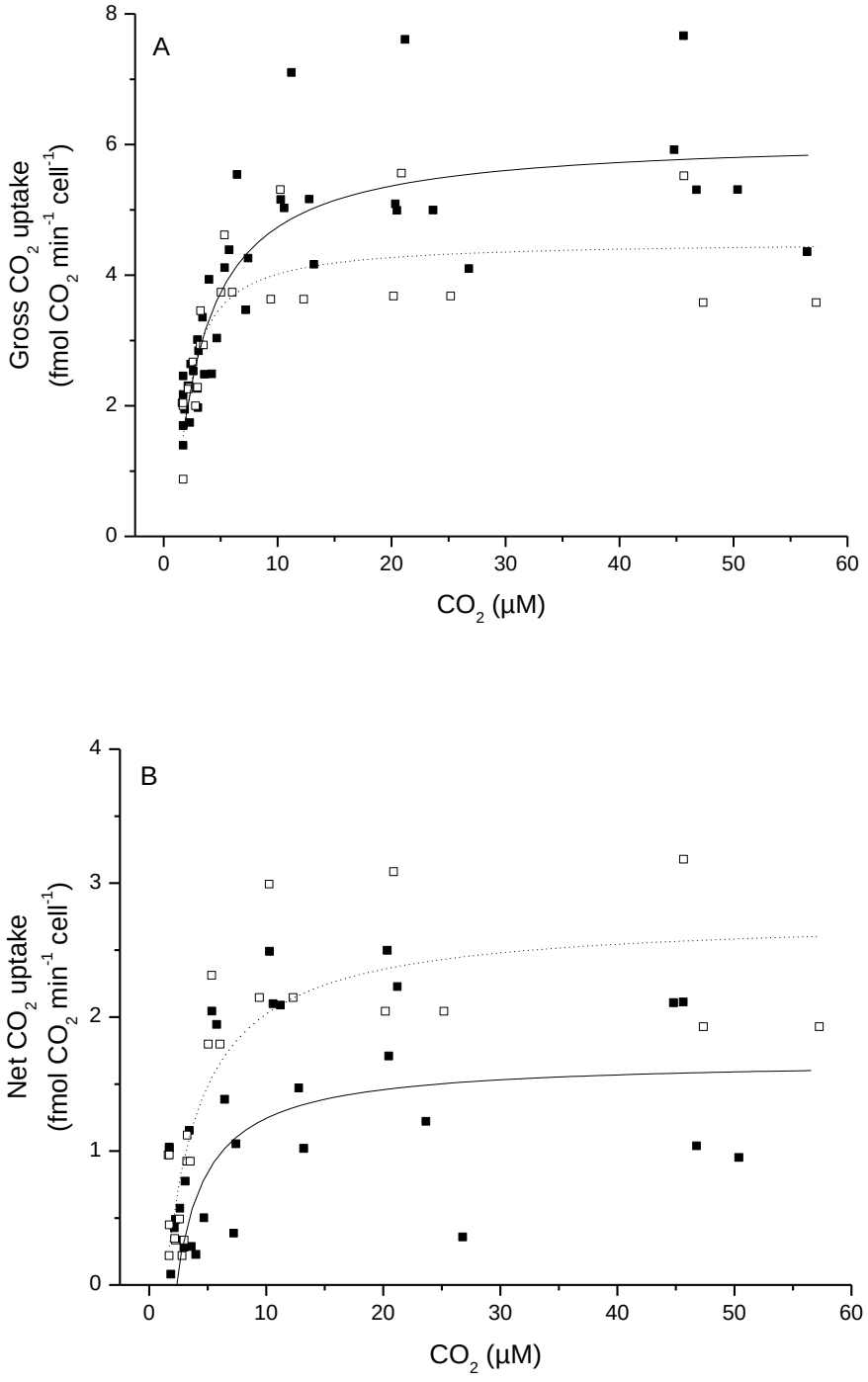

Figure 25. Kinetics of gross CO_2 (A) and net CO_2 (B) uptake in cells grown under high (■) and low (□) NO_3^-. For gross and net CO_2 uptake in cells grown under high (H) NO_3^- (n=5). All other values represent the means of triplicates.

4. Discussion

The aim of the present study was to investigate how cells regulate C and N fluxes and to determine the relative composition of macromolecular pools in response to NO_3^- availability in *E. huxleyi*. Despite of similar growth rates and C to N ratios the allocation of fixed C and N changes with NO_3^- supply.

4.1. Growth parameters

The response of cells to different N availability generally depends on the degree of limitation. The aim of the present study was to impose moderate N limitation in cells of *E. huxleyi* and as a result, growth rates did not change much in response to NO_3^- availability (Tab. IV). However, low NO_3^--grown cells reduced C as well as N quotas (Tab. IV). As a consequence, C and N production were lower under low NO_3^- (Fig. 9a and 9b). N limitation was also indicated by decreasing volume and protein content per cell under low NO_3^- (Tab. IV). Indeed, microalgae are able to maintain high growth rates during the onset of N limitation (Giordano et al., 2001) and are able to respond to the large variation of N cell quota (Parslow et al., 1984; Borchardt et al., 1996) similar to cells in our study. Maintaining high growth rates during the onset of N limitation may also be among other factors attributing to the capacity of intracellular NO_3^- storage, which occurs in various phytoplankton cells (Dortch 1982; Stolte and Riegmann, 1995; McGlathery et al., 1996). This storage mechanism has not been studied yet for *E. huxleyi* and thus, we cannot make any suggestions about a possible intracellular NO_3^- storage in cells of our study.

The number of visible coccoliths per cell did not change and the percentage of incomplete coccoliths, which contain less calcite than normal coccoliths strongly increased due to N

limitation (Fig. 10; Fig. 11). Thus, we infer that the reduced cellular inorganic C content and inorganic C production were likely caused by a reduced inorganic C content per coccolith. However, a diminished calcite content of coccoliths produced under N limitation was observed in a chemostat-experiment using *E. huxleyi* (Paasche, 1998). The author also noted that coccoliths produced under N limitation were smaller than coccoliths produced under N repletion and he described the morphology of the former as "undercalcified". These observations are in line with our findings. Paasche (1998) also reported a lower Ca^{2+} content in coccoliths of N limited cells, but unfortunately we did not measure the Ca^{2+} content in coccoliths of cells in our study.

4.2. Macromolecular pools

Nitrate availability had also an impact on the C and N macromolecular pools in *E huxleyi*. Low NO_3^--grown cells had a lower ratio of proteins to lipids whereas the ratios of proteins to carbohydrates and lipids to carbohydrates increased compared to cells under high NO_3^- (Fig. 12). Similar results in the ratios of macromolecular pools have been also obtained for N limited cells of the marine diatom *Chaetocheros muellerii* by Giordano et al. (2001).

Giordano et al. (2001) reported that proteins belong to the primary cell compounds, which are reduced due to low NO_3^- availability and ongoing N limitation. Such changes can be explained by the constant growth rates (continuous cell divisions) in combination with the low NO_3^-availability and the decline in cellular components by new biomass production (McGlathery et al., 1996). Among proteins, RubisCO is the most abundant in photosynthetic organisms and the reduction in the amount of RubisCO as well as of its activity is well established in algae under N limitation (Falkowski et al., 1989; Beardall, 1991; Young and Beardall, 2005). Moreover, N limitation was found to cause a rearrangement of intracellular

pools (McGlathery et al., 1996) driving carbon away from protein synthesis and relocating it into lipids (Giornano et al., 2001).

4.3. Nitrate assimilation

Growing either under high or low NO_3^-, cells are able to maintain constant C to N ratio by regulating their N assimilation according to the N availability. Under low NO_3^-, cells had lower NR and NiR V_{max} compared to those grown under high NO_3^- conditions (Tab. V). This effect is attributed to the decrease of cell volume and cell protein under low NO_3^- because NR and NiR V_{max} are quite similar in the two NO_3^- treatments when enzyme activities are expressed on a per cell volume or cell protein basis. Since the genes coding for NR and NiR are located in the same gene cluster as has been previously reported for *C. reinhardtii* (Quesada et al, 1998), low NO_3^-should lead to lower expression of NR and NiR mRNA in *E. huxleyi* cells thereby decreasing the NR and NiR protein contents and activities. We did not observe any significant modification in the K_m (NADH) of NR for this substrate under high or low NO_3^- (Tab. V). The findings make sense because NADH is not expected to become a limiting factor at high light intensities under which cells of both NO_3^- treatments were acclimated. Nevertheless, the affinities of NR for NO_3^- and NiR for NO_2^- are higher under low NO_3^- (Tab. V) indicating a more efficient reduction of NO_3^- to NH_4^+ in these cells. The cellular mechanism(s) responsible for the increase of the catalytic efficiency of NR and NiR under low NO_3^- is (are) not known. 14-3-3 proteins may be involved in his type of regulation, since they were found to play a role in regulating protein activity and turnover rate (Korkhout et al., 1994; Oeckling et al., 1997; Weiner and Kaiser, 1999). Whether 14-3-3 proteins are involved in regulating the catalytic efficiencies of NR and NiR in *E. huxleyi* and whether they

are responsible for higher affinities of NO_3^- and NO_2^- reduction under low NO_3^- or not have still to be tested.

Maintaining constant C to N ratio under high and low NO_3^- also includes the regulation of the enzymes in the GS/GOGAT cycle where C and N assimilation meet. Irrespective of the type of normalization, GS V_{max} was found to be higher in low NO_3^--grown cells (Tab. VI). This increase in GS V_{max} in cells under low NO_3^- might be due to GS_2 activity, which was found to be higher than GS_1 activity in these cells (Fig. 18b). The amount of the GS_2 isoform was not affected by NO_3^- availability in cells of *E. huxleyi* despite the difference in GS_2 specific activity between the different NO_3^- treatments (Fig. 19; Tab. VII). This finding agrees with the study of Chen and Silflow (1996), who reported that the level of GS_2 transcripts was unaffected by NO_3^- availability in *C. reinhardtii*. The same authors also showed that the level of GS_1 transcripts in *C. reinhardtii* is induced by NO_3^-. This may explain the lower amount and activity of the GS_1 isoform in cells at 10 µM NO_3^- compared with cells grown at 280 µM NO_3^- (Fig. 20, Fig. 21, Tab. VII). The increase of GS activity in microalgae has been attributed to light activation due to reduction of the enzyme by reduced thioredoxin but also to de novo biosynthesis of GS protein during the light period (Tischner and Hüttermann, 1980; Schmidt, 1981; Tischner and Schmidt, 1982; Florencio et al., 1993). Besides, the increase in GS V_{max}, GS affinity for Glu was higher in low NO_3^--grown cells whereas enzyme affinities for ATP and NH_2OH remained similar in cells of the two NO_3^- treatments (Tab. VI). This difference in the affinity for Glu may be related to the proportion and the affinity for Glu of each of the GS isoform in the tested NO_3^- concentrations. Unfortunately we could not conduct a kinetic analysis on the two isoforms due to low cell densities in order to evaluate the affinity of GS_1 and GS_2 for Glu. 14-4-3 proteins could also play a role in the regulation of GS

catalytic activity (Moorhead et al., 1999; Finnemann and Schjoerring, 2000), but this type of regulation has not been tested yet in *E. huxleyi*.

As expected, GOGAT activity showed more or less the same response with GS activity to NO_3^- availability since both enzymes are part of the same cycle (Tab. VI). As in the case of total GS, the higher activity of GOGAT at 10 μM NO_3^- may be due to regulation in the protein level by thioredoxin (Tischner and Schmidt, 1982).The lower PEPCK activity observed at 10 μM NO_3^- (Tab. VI) likely reflects the need of these cells to match the flow of C into amino acid synthesis with the flow of N under these conditions.

4.4. Photosynthesis and respiration

Net photosynthesis per cell and Chl *α* decreased in cells under low NO_3^- (Tab. VIII). When expressed per cell chlorophyll, photosynthetic rates were similar in the two NO_3^- treatments. While low NO_3^- availability decreases the amount of chlorophyll and the rate of photosynthesis per cell, higher affinities of photosynthesis for CO_2 and DIC were measured in low NO_3^--grown cells (Tab. VIII). Lower rates of photosynthesis may be related primarily to the composition of PSI and PSII in terms of integral proteins and pigments, and secondly to the abundance and regulation of proteins, which receive most of the reductant (NADPH) and ATP produced by photosynthesis such as Rubisco. Indeed, N limitation leads to increased ratios of carotenoids to Chl *α*, causes a reduction in thylakoid stacking and absorptivity and decreases the amount of Rubisco per cell in algae (Plumley et al., 1989; Falkowksi et al., 1989; Beardall et al., 1991). Furthermore, despite of the onset of N limitation the apparent chlorophyll-specific efficiency of light harvesting (α) in low NO_3^--grown cells was similar with the one under high NO_3^- (Tab. VIII). Previous experiments showed that N limitation may

increase, decrease or maintain α (Osborne and Geider, 1986; Kolber et al., 1988; Herzig and Falkowski, 1989) depending on the investigated species as well as the degree of N limitation.

In contrast to photosynthesis, the rate of respiration per cell was similar between high and low NO_3^--grown cells (Tab. VIII), but was higher in low NO_3^--grown cells when expressed on cell chlorophyll. Under low NO_3^-, respiration may compensate for the lower amount of reductant and ATP provided by photosynthesis in these cells. Weber and Turpin (1989) reported that the reductant deriving from photosynthesis is not sufficient enough to meet the demands of NO_3^- and NO_2^- reduction in N-limited cells of *S. minutum* and this deficiency in reducing power is compensated by TCA cycle reductant. The measured respiration rates in low NO_3^--grown cells may also be related to higher rates of N assimilation in the dark compared to cells under high NO_3^-. It has been shown that respiration increases in the dark, in order to support N assimilation in the green alga *S. minutum* (Vanlerberghe et al., 1992).

4.5. Inorganic carbon uptake

Cells of *E. huxleyi* change their preference of inorganic C species with respect to N availability. At low NO_3^-, cells down regulated HCO_3^- uptake compared to cells grown at high NO_3^- (Tab. VIII), probably as a result of less HCO_3^- transporters in these cells due to the lower NO_3^- availability. The increase in the affinity of HCO_3^- transport in cells at low NO_3^- may be related to a direct interaction of 14-3-3 proteins with the HCO_3^- transporters, or to an indirect interaction of 14-3-3 proteins with the H^+-ATPase (Korkhout et al., 1994; Oeckling et al., 1997), which is essential for proton transport across membranes. Despite the smaller size of cells at low NO_3^-, gross CO_2 uptake (uptake of CO_2 into the cell) and net CO_2 uptake (gross CO_2 uptake minus CO_2 efflux) were similar in cells of both NO_3^- treatments (Tab. VIII). This

response in CO_2 uptake, in combination to the higher affinity for CO_2 in cells at low NO_3^- (Tab. III), can be related to the regulation of proteins, which utilize CO_2 such as RubisCO and/or carbonic anhydrase (CA). Again, phosphorylation and interaction with 14-3-3 proteins may be the reason for higher affinities for CO_2 in cells grown at low NO_3^-.

4.6. Intracellular concentrations of nitrate and carbon dioxide

Based on the enzyme kinetics measured for NR and the kinetics of net photosynthesis derived from the MIMS measurements, we estimated the intracellular concentrations of NO_3^- and CO_2 which allows for balanced growth, i.e. maintenance of a constant C to N ratio. Under these circumstances, the net fixation rate of C (C_{flux}) can thus be expressed in terms of the N assimilation rate (N_{flux}), using the C to N ratio:

$$\frac{C_{flux}}{N_{flux}} = \frac{POC}{PON} \quad (1)$$

The upper boundary for C_{flux} in balance with N assimilation is provided by the maximum NR activity (V_{max}^{NR}) and would be obtained at infinite NO_3^- concentration in the cytosol. Using our result for V_{max}^{NR}, the upper limit for C_{flux} that derives from equation (1) is very similar to the maximum net photosynthesis (in terms of C), which we obtained from the MIMS measurements ($V_{max}^{CO_2} = V_{max}^{O_2}/PQ$, with PQ being the photosynthetic quotient). For balanced growth to be maintained (equation 1), the upper limit for C_{flux} must assume a value of 9.3 fmol min^{-1} $cell^{-1}$ for the high NO_3^- condition (POC/PON = 8.5), and 5.3 fmol min^{-1} $cell^{-1}$ for cells acclimated to the low NO_3^- concentration (POC/PON = 8.3). Given the photosynthetic quotient from a NO_3^--utilizing cell (PQ=1.36; Williams and Robertson, 1991), the MIMS measurements predict a $V_{max}^{CO_2}$ of 9.5 ± 0.5 fmol min^{-1} $cell^{-1}$ and 4.8 ± 0.6 fmol min^{-1} $cell^{-1}$, for

the high and low NO_3^- conditions, respectively. Hence, the ratios of $V_{max}^{CO_2}$ and V_{max}^{NR} are approximately given by the C to N ratios for the two growth NO_3^- concentrations used for this study (high NO_3^-: 1.0 POC/PON, low NO_3^-: 0.9 POC/PON). Using equation (1) and $V_{max}^{CO_2} / V_{max}^{NR} \approx$ POC/PON it follows that

$$\frac{C_{flux}}{V_{max}^{CO_2}} \approx \frac{N_{flux}}{V_{max}^{NR}} \quad (2)$$

Finally, we assumed for the C_{flux} the enzyme activity of RubisCO and for the N_{flux} the enzyme activity of NR. Then, equation (2) yields the condition for balanced growth in terms of the intracellular concentrations of NO_3^- and CO_2

$$\frac{CO_2}{K_{Rub}} \approx \frac{\left[NO_3^-\right]}{K_{NR}} \quad (3)$$

with K_{Rub} and K_{NR} being the Michaelis-Menten constant for RubisCO and NR, respectively. Generally, for an enzyme possessing the activity V_0, the ratio of the concentration of the substrate S and the Michaelis-Menten constant Km determines the degree of saturation of the enzyme activity ($V_0/V_{max}=1/(Km/[S]+1)$). Based on equation (3) it follows that a constant C to N ratio can be maintained for intracellular concentrations of CO_2 and NO_3^- which yield a comparable saturation of the enzyme activity for the enzymes involved in C and N assimilation. Hence, the maintenance of a constant C to N ratio requires a concerted regulation of the intracellular [CO_2] and [NO_3^-] to equilibrate the fluxes through the C and N assimilation pathway. It should be noticed that equation (3) is valid for all degrees of enzyme saturation ($0 < V_0/V_{max} < 1$) in the cells acclimated to the two growth regimes. For instance, when the NR activity reaches 80% of its maximum value, NO_3^- accumulates in the cytosol, yielding concentrations of 396 µM and 296 µM for the cells acclimated to high and low NO_3^-, respectively. For balanced growth to be maintained (equation (3)), the CO_2 concentration at

the site of RubisCO must then exceed K_{Rub} by a factor of 4, for the high and low NO_3^- conditions. The values of K_{Rub} for the two growth conditions are not known. Assuming a K_{Rub} of 30 µM (Badger et al., 1998), it follows a $[CO_2]$ at RubisCO of 120 µM. We assumed steady state conditions for N assimilation. In other words, the substrates inside the cell accumulate until the rates of reactions are the same for all the enzymes involved in the N assimilation pathway (from NO_3^- to NH_4^+ assimilation by GS):

$$N_{flux} = \frac{V_{max}^{NR}\left[NO_3^-\right]}{K_{NR}+\left[NO_3^-\right]} = \frac{V_{max}^{NiR}\left[NO_2^-\right]}{K_{NiR}+\left[NO_2^-\right]} = \frac{V_{max}^{GS}\left[NH_4^+\right]}{K_{GS}+\left[NH_4^+\right]} \quad (4)$$

Then, the NiR kinetics data predicts an accumulation of high NO_2^- concentrations at the site of NiR activity. Similar K_m values of NiR for NO_2^- have been also reported for the flagellate *Prorocentrum minutum* and internal NO_2^- pools were 4 to 5 mM in the diatom *Chaetocheros* sp. (Lomas and Glibert, 2000). The requirement for a high NO_2^- concentration for *E. huxleyi* NiR is suggestive of the fact that this enzyme is confined in the proximity of the chloroplast envelope, possibly near the entry point of NO_2^- into the chloroplast. The V_{max} of NiR and GS are probably underestimated due to suboptimal conditions caused by the sample preparation and the pH optimum of the enzymes. GS activity was found to be ca. 40% higher when measured with a radioactive assay with ammonia as substrate in comparison to the colorimetric assay with NH_2OH as substrate (Listrom et al., 1997) and therefore cannot be used to estimate intracellular NH_4^+ concentrations.

4.7. Conclusions

In conclusion, NO_3^- availability seems to have a crucial impact on the regulation of C and N fluxes in the marine coccolithophore *E. huxleyi*, without necessarily changing the C to N ratios and/or growth rates of cells. With the exception of GS and GOGAT, cells generally respond to low NO_3^- availability with a down-regulation of activities of proteins involved in the acquisition and assimilation of inorganic C and N. Simultaneously, the substrate affinities of these proteins increase in response to low NO_3^-. This study indicates that the intracellular CO_2 and NO_3^- concentrations near RubisCO and NR have to be carefully regulated in order to equilibrate the fluxes through the C and N assimilation pathways, thus ensuring adequate growth under the respective NO_3^- conditions. Decreasing NO_3^- availability in the future ocean due to increased stratification of the upper water masses will decrease marine primary production and microalgae cells, such as the coccolithophore *E. huxleyi*, by reduction of individual size. Nevertheless, NO_3^- availability does not affect the PIC to POC ratio in *E. huxleyi* cells, as long as growth rates and C to N ratios remain constant, and have putatively no significant effect in the biologically mediated ocean-atmosphere CO_2 exchange.

5. Literature cited

Badger MR, Palmqvist K, Yu JW (1994) Measurement of CO_2 and HCO_3^- fluxes in cyanobacteria and microalgae during steady-state photosynthesis. Physiol Plant **90**: 529-536

Badger MR, Andrews TJ, Whitney SM, Ludwig M, Yellwolees C, Leggat W, Price GD (1998) The diversity and coevolution of Rubisco, plastids, pyrenoids, and chloroplast-based CO_2-concentrating mechanisms in microalgae. Can J Bot **76**: 1052-1071

Baumann KH, Bockel B, Frenz M (2004) Coccolith contribution to South Atlantik carbonate sedimentation. In HR Thierstein, JR Young, eds, Coccolithophores: From Molecular Processes to Global Impact, Springer, Berlin, pp 367-402

Beardall J, Raven J (1990) Pathways and mechanisms of respiration in microalgae. Mar Microb Food Webs **4**: 7–30

Beardall J, Roberts S, Millhouse J (1991) Effects of nitrogen limitation on uptake of inorganic carbon and specific activity of ribulose-1,5-bisphosphate carboxylase/oxygenase in green microalgae. Can J Bot **69**: 1146-1150

Beardall J, Johnston A, Raven JA (1998) Environmental regulation of CO_2-concentrating mechanisms in microalgae. Can J Bot **76**: 1010-1017

Beardall J, Giordano M (2002) Ecological implications of microalgal and cyanobacterial CO_2 concentrating mechanisms, and their regulation. Funct Plant Biol **29**: 335-347

Berges JA, Harrison PJ (1995) Relationships between nitrate reductase activity and rates of growth and nitrate incorporation under steady-state light or nitrate limitation in the marine diatom *Thalassiosira pseudonana*. J Phycol **31**: 85-95

Birch DG, Elfiri IR, Turpin DH (1986) Nitrate and ammonium induced photosynthetic suppression in N-limited *Selenastrum minutum*. II. Effects of NO_3^- and NH_4^+ addition on CO_2 efflux in the light. Plant Physiol **82**: 708-712

Borchardt MA 1996. Nutrients. In RJ Stevenson, RL Lowe, ML Bothwell, eds, Algal Ecology: Freshwater Benthic Ecosystems, Academic Press, London, pp 183-227

Bradford MM (1976) A rapid and sensitive method for the quantitation of microgram quantities of protein utilizing the principle of protein-dye binding. Anal Biochem **72**: 248-254.

Brewer PG, Bradshaw AL, Williams RT (1986) Measurement of total carbon dioxide and alkalinity in the North Atlantic Ocean in 1981. In DE Reichle, eds, The global carbon cycle: Analysis of the natural cycle and implications of anthropogenic alterations for the next century, New York, Springer, pp 358-381

Carpenter EJ (1983) Nitroegn fixation by marine *Oscillatoria* (Tricodesmium) in the world´s ocean. In Carpenter EJ, Capone DG, (eds), Nitrogen in the marine environment. Academic Press, pp 1-37

Capone DG (1983) Benthic nitrogen fixation. In Carpenter EJ, Capone DG, (eds), Nitrogen in the marine environment. Academic Press, pp 1-37

Chen Q, Silflow CD (1996) Isolation and characterization of glutamine synthetase genes in Chlamydomonas reinhardtii. Plant Physiol **112**: 987-996

Cullimore JV, Sims AP (1981) Glutamine sythetase of *Chlamydomonas*: its role in the control of nitrate assimilation. Planta **153**: 18-24

Dickson AG, Millero FJ (1987) A comparison of the equilibrium constants for the dissociation of carbonic acid in seawater media. Deep Sea Res **34**: 1733-1743

Domenighini A, Giordano M (2009) Fourier transform infrared spectroscopy of microalgae as a novel tool for biodiversity studies, species identification, and the assessment of water quality. J Phycol **45**: 522-531

Dortch Q (1982) Effect of growth conditions on accumulation of internal nitrate, ammonium, amino acids and protein in three marine diatoms. J Exp Mar Biol Ecol **61**: 243-264

Dugdale RC (1967) Nutrient limitation in the sea: Dynamics, identification and significance. *Limnol Oceanogr* **12**: 685-695

Dugdale RC, Goering JJ (1967) Uptake of new and regenerated forms of nitrogen in primary production. Limnol Oceanogr **12**: 196-206

Elfiri IR, Turpin DH (1986) NO_3^- and NH_4^+ induced photosynthetic suppression in N-limited *Selenastrum minutum*. Plant Physiol **81**: 273-279

Elfiri IR, Turpin DH (1987) The path of carbon flow during NO_3^--induced photosynthetic suppresion in N-limited *Selenastrum minutum*. Plant Physiol **83**: 97-104

Falkowski PG, Sukenik A, Herzig R (1989) Nitrogen limitation in *Isochrysis galbana* (Haptophyceae). II. Relative abundance of chloroplast proteins. J Phycol **25**: 471-478

Fernandez E, Galvan A (2007) Inorganic nitrogen assimilation in *Chlamydomonas*. J Exp Bot **58**: 2279-2287

Finnemann J, Schjoerring JK (2000) Post-translational regulation of cytosolic glutamine synthetase by reversible phosphorylation and 14-3-3 protein interaction. Plant J **24**: 171-181

Florencio FJ, Gadal P, Buchanan BB (1993) Thioredoxin-linked activation of the chloroplast and cytosolic forms of *Chlamydomonas reinhardtii* glutamine synthetase. Plant Physiol Biochem **31**: 649-655

Fritz JJ 1999. Carbon fixation and coccolith detachment in the coccolithophore *Emiliania huxleyi* in nitrate-limited cyclostats. Mar Biol **133**: 509-518

Galvan A, Cordoba F, Cardenas J, Fernandez E (1991) Regulation of nitrite uptake and nitrite reductase expression in *Chlamydomonas reinhardtii*. Biochim Biophys Acta **1074:** 6–11

Galvan A, Quesada A, Fernandez E (1996) Nitrate and nitrite are transported by different specific transport systems and by a bispecific transporter in *Chlamydomonas reinhardtii*. J Biol Chem **271**: 2088-2092

Galvan A, Fernandez E (2001) Eukaryotic nitrate and nitrite transporters. Cell Mol Life Sci **58**: 225-233

Galvan A, Rexach J, Mariscal V, Fernandez E (2002) Nitrite transport to the chloroplast in *Chlamydomonas reinhardtii*: molecular evidence for a regulated process. Journal of Exp Bot **53**: 845–853

Giordano M, Kansiz M, Heraud P, Beardall J, Wood B, McNaughton D (2001) Fourier trnsform infrared spectroscopy as a novel tool to investigate changes in intracellular macromolecular pools in the marine microalga *Chaetoceros muellerii* (Bacillariophyceae). J Phycol **37**: 271-279

Giordano M, Beardall J, Raven JA (2005a) CO_2 concentrating mechanisms in algae. Mechanisms, environmental modulation, and evolution. Annu Rev Plant Biol **56**: 99-131

Giordano M, Chen YB, Koblizek M, Falkowski P (2005b) Regulation of nitrate reductase in *Chlamydomonas reinhardtii* by the redox state of the plastoquinone pool. Eur J Phycol **40**: 345-352

Gran G 1952. Determinations of the equivalence point in potentiometric titrations of seawater with hydrochloric acid. Oceanol Acta **5**: 209-218

Guillard RRL, Ryther JH (1962) Studies of marine planktonic diatoms. Can J Microbiol **8**: 229-239

Herzig R, Falkowski PG (1989) Nitrogen limitation in *Isochrysis galbana* (Haptophyceae). I. Photosynthetic energy conversion and growth efficiencies. J Phycol **25**: 462-471

Hipkin CR, Thomas RJ, Syrett PJ (1983) Effects of nitrogen deficiency on nitrate reductase, nitrate assimilation and photosynthesis in unicellular marine algae. Mar Biol **77**: 101-107

Holdsworth ES, Bruck K (1977) Enzymes concerned with β-carboxylation in marine phytoplankter: Purification and properties of phosphoenolpyruvate carboxykinase**.** Arch Biochem Biophys **182**: 87-94

Houghton JT, Meira Filho LG, Callander BA, Harris N, Kattenberg A, Maskell K (1995) Climate Change 1995: The Science of Climate Change. Contribution of Working Group I to the Second Assessment Report of the Intergovernmental Panel of Climate Change, Cambridge Univ. Press, Cambridge, UK and New York, USA

Howarth RW (1988) Nutrient limitation of net primary production in marine ecosystems. Ann Rev Ecol **19**: 89-110

Huppe HC, Turpin DH (1994) Integration of carbon and nitrogen metabolism in plant and algal cells. Annu Rev Plant Physiol **45**: 577-607

Ietswaart T, Schneider PJ, Prins RA (1994) Utilization of organic nitrogen sources by two phytoplankton species and a bacterial isolate in pure and mixed culture. Appl Environ Microb **60**: 1554-1560

Iglesias-Rodriguez MD, Halloran PR, Rickaby REM, Hall IR, Colmenero-Hidalgo E, Gittins JR, Grenn D RH, Tyrrell T, Gibbs SJ, von Dassow P, Rehm E, Armbrust EV, Boessenkool KP (2008) Phytoplankton calcification in a high-CO_2 world. Science **320**: 336-340

Iwamoto K, Shiraiwa Y (2003) Characterization of NADH: nitrate reductase from the coccolithophorid *Emiliania huxleyi* (Lohman) Hay & Mohler (Haptophyceae). Mar Biotechnol **5**: 20-26

Johnston AM, Raven JA (1989) Extraction, partial purification and characterization of phosphoenolpyruvate carboxykinase from *Ascophyllum nodosum*. (Phaeophyceae). J Phycol **25**: 568-576

Kanda J (1995) Nitrate assimilation and new production in open ocean. *In* Sakai, H. & Nozaki, Y. [Eds.] *Biogeochemical Processes and Ocean Flux in the Western Pacific*. Terra Scientific Publishing Company (TERRAPUB), Tokyo, pp.227-238

Kiefer DA (1983) Chlorophyll a fluorescence in marine centric diatoms: response of chloroplast to light and nutrient stress. Mar Biol **23**: 39-46

Kolber A, Zehr J, Falkowski P (1988) Effects of growth irradiance and nitrogen limitation on photosynthetic energy conversion in photosystem II. Plant Physiol **88**: 923-929

Korkhout HAAJ, de Boer A (1994) A fusicoccin binding protein belongs to the family of 14-3-3 brain protein homologs. Plant Cell **6**: 1681-1692

Laemmli UK (1970) Cleavage of structural proteins during the assembly of the head of bacteriophage T4. Nature **227**: 680-685

Lapointe BE, Duke CS (1984) Biochemical strategies for growth of *Gracilaria tikvahiae* (Rhodophyta) in relation to light intensity and nitrogen availability. J Phycol **20**: 488-495

Lea PJ, Robinson SA, Stewart GR (1990) The enzymology and metabolism of glutamine, glutamate and asparagines. In BJ Miflin, PJ Lea, eds, The Biochemistry of Plants, Vol. 16. Academic Press, San Diego, pp 121-159

Lea PJ (1993) Nitrogen metabolism. In Lea PJ, Leegood RC, eds, Plant Biochemistry and Molecular Biology, John Wiley and Sons, pp 155-181

Lewis E, Wallace DWR (1998) Program developed for CO_2 system calculations. ORNL/CDIAC-105. Carbon dioxide information analysis center, Oak Ridge National laboratory, U.S. Department of Energy

Lin CC, Kao CH (1996) Disturbed ammonium assimilation is associated with growth inhibition of roots in rice seedlings caused by NaCl. Plant Growth Reg **18**: 233-238

Lindschooten C, van Bleijswijk JDL, van Emberg PR, de Vrind JPM., Kempers ES, Westbroek P, de Vrind-de Jong EW (1991) Role of the light-dark cycle and medium composition on the production of coccoliths by *Emiliania huxleyi* (Haptophyceae). J Phycol **27**: 82-86

Listrom CD, Morizono H, Rajagopal BS, McCann MT, Tuchman M, Allewell NM (1997) Expression, purification, and characterization of recombinant human glutamine synthetase. Biochem J **328**: 159-163

Lomas MW, Glibert PM (2000) Comparisons of nitrate uptake, storage, and reduction in marine diatoms and flagellates. J Phycol **36**: 903-913

Mariscal V, Moulin P, Orsel M, Miller AJ, Fernandez E, Galvan A (2006) Differential regulation of the *Chlamydomonas Nar1* gene family by carbon and nitrogen. Protist **157**: 421–433

Maurin C, Le Gal Y (1997a) Isoforms of glutamine synthetase in the marine coccolithophorid *Emiliania huxlyei* (Prymnesiophyceae). Comp Biochem Physiol **118**: 903-912

Maurin C, Le Gal Y (1997b) Glutamine synthetase in the marine coccolithophorid *Emiliania huxleyi* (Prymnesiophyceae): regulation of activity in relation to light and nitrogen availability Plant Science **122**: 61-69

Maurin-Defossez C, Le Gal Y (1998) Diel periodicity of glutamine synthetase activity during the cell cycle of *Emiliania huxleyi*. Plant Physiol Biochem **36**: 233-236

McGlathery KJ, Pedersen FM, Borum J (1996) Changes in intracellular nitrogen pools and feedback controls on nitrogen uptake in *Chaetomorpha linum* (Chlorophyta). J Phycol **32**: 393-401

Menacho A, Vega MV (1989) Effect of nitrogen starvation on ammonium assimilation by *Chlamydomonas reinhardtii*. Physiol Plant **75**: 285-289

Mehrbach C, Culberson C, Hawley J, Pytkovycz R (1973) Measurement of the apparent dissociation constants of carbonic acid in seawater at atmospheric pressure. Limnol Oceanogr **18**: 897-907

Mitra M, Lato SM, Ynalvez RA, Xiao Y, Moroney JV (2004) Identification of a new chloroplast carbonic anhydrase in *Chlamydomonas reinhardtii*. Plant Physiol **135**: 173-182

Moorhead G, Douglas P, Cotelle V, Harthill J, Morrice N, Meek S, Deiting U, Stitt M, Scarabel M, Aitken A, MacKintosh C (1999) Phosphorylation-dependent interactions between enzymes of plant metabolism and 14-3-3 proteins. Plant J **18**: 1-12

Navarro MT, Prieto R, Fernandez E, Galvan A (1996) Constitutive expression of nitrate reductase changes the regulation of nitrate and nitrite transporters in *Chlamydomonas reinhardtii.* Plant J **9:** 819–827

Norici A, Dalsass A, Giordano M (2002) Role of phosphoenolpyruvate carboxylase in anaplerosis in the green microalga *Dunaliella salina* cultured under different nitrogen regimes. Physiol Plant **116**: 186-191

Oaks A, Stulen I, Jones K, Winspear MJ, Misra S, Boesel IL (1980) Enzymes of nitrogen assimilation in maize roots. Planta **148**: 477-484

Oeckling C, Piotrowski M, Hagemeier J, Hagemann C (1997) Topology and target interaction of the fusicoccin-binding 14-3-3 homologs of *Commelina communis*. Plant J **12**: 441-453

O´Neal D, Joy KW (1973) Glutamine synthetase of pea leaves. I. Purification, stabilization and pH optima. Arch Biochem Biophys **159**: 113-122

Osborne BA, Geider RJ (1986) Effect of nitrate-nitrogen limitation on photosynthesis of the diatom *Phaeodactylum tricornutum* Bohlin (Bacillariophyceae). Plant Cell Environ **9**: 617-625

Paasche E 1998. Roles of nitrogen and phosphorus in coccolith formation in *Emiliania huxleyi* (Prymnesiophyceae). Eur J Phycol **33**: 33-42

Page S, Hipkin CR, Flynn KJ (1999) Interactions between nitrate and ammonium in *Emiliania huxleyi***.** J Exp Mar Biol Ecol **236**: 307-319

Palenik B, Henson SE (1997) The use of amides and other organic nitrogen sources by the phytoplankton *Emiliania huxleyi*. Limnol Oceanogr **42**: 1544-1551

Parslow JS, Harrison PJ, Thomson PA (1984) Saturated uptake kinetics: transient response of the marine diatom *Thalassiosira pseudonana* to ammonium, nitrate, silicate or phosphate starvation. Mar Biol **83**: 51-59

Plumley FG, Douglas SE, Switzer AB, Schmidt GW (1989) Nitrogen-dependent biogenesis of chlorophyll-protein complexes. In WR Briggs, eds, Photosynthesis. Allan R. Liss Inc., New York, pp 311-329

Quesada A, Fernandez E (1994) Expression of nitrate assimilation related genes in *Chlamydomonas reinhardtii*. Plant Mol Biol **24**: 185-194

Quesada A, Galvan A, Fernandez E (1994) Identification of nitrate transporter genes in *Chlamydomonas reinhardtii*. Plant J **5**: 407-419

Quesada A, Gomez I, Fernandez E (1998) Clustering of the nitrite reductase gene and a light-regulated gene with nitrate assimilation loci in *Chlamydomonas reinhardtii*. Planta **206**: 259-265

Raven JA, Johnston AM (1991) Mechanisms of inorganic carbon acquisition in marine phytoplankton and their implications for the use of other resources. Limnol Oceanogr **36**: 1701-1714

Raven JA (1997) Inorganic carbon acquisition in marine autotrophs. Adv Bot Res **27**: 85-209

Rees AP, Malcolm E, Woodward S, Joint I (2006) Concentrations and uptake of nitrate and ammonium in the Atlantic Ocean between **60°N** and **50°S**. Deep Sea Res **53** (14-16): 1649-1665

Reinfelder JR, Kraepiel AML, Morel FMM (2000) Unicellular C_4 photosynthesis in a marine diatom. Nature **407**: 996-999

Reinfelder JR, Milligan AJ, Morel FMM (2004) The role of the C_4 pathway in carbon accumulation and fixation in a marine diatom. Plant Physiol **135**: 2106-2111

Rexach J, Montero B, Fernandez E, Galvan A (1999) Differential regulation of the high affinity nitrite transport systems III and IV in *Chlamydomonas reinhardtii*. J Biol Chem **274**: 27801-27806

Rexach J, Fernandez E, Galvan A (2000) The *Chlamydomonas reinhardtii Nar1* gene encodes a chloroplast membrane protein involved in nitrite transport. Plant cell **12**: 1441-1453

Rhiel E, Morschel E, Wehrmeyer W (1985) Correlation of pigment deprivation and ultrastructural organization of thylakoid membranes in *Cryptomonas maculata* following nutrient deficiency. Protoplasma **129**: 62-73

Rhiel E, Krupinska K, Wehrmeyer W (1986) Effects of nitrogen starvation on the function and organization of the photosynthesis membranes in *Cryptomonas maculata* (Cryptophyceae). Planta **169**: 361-369

Riegmann R, Stolte W, Noordeloos AAM, Slezak D (2000) Nutrient uptake and alkaline phosphatase activity of *Emiliania huxleyi* (Prymnesiophyceae) during growth under N and P limitation in continuous cultures. J Phycol **36**: 87-96

Rost B, Riebesell U, Burkhardt S, Sültemeyer D (2003) Carbon acquisition of bloom-forming marine phytoplankton. Limnol Oceanogr **48**: 55-67

Rost B, Riebesell U (2004) Coccolithophores and the biological pump: responses to environmental changes**.** Coccolithophores : from molecular processes to global impact / Hans R. Thierstein; Jeremy R. Young (Eds.) Berlin [u.a.] : Springer, 99-125

Rost B, Riebesell U, Sültemeyer D (2006). Carbon acquisition of marine phytoplankton: Effect of photoperiod length. Limnol Oceanogr **51**: 12-20

Rost B, Kranz SA, Richter K-U, Tortell PD (2007**)** Isotope disequilibrium and mass spectrometric studies of inorganic carbon acquisition by phytoplankton. Limnol Oceanogr Methods **5**: 328-337

Sharp JH (1983) The distributions of inorganic nitrogen and dissolved and particulate organic nitrogen in the sea. In Carpenter EJ, Capone DG, (eds), Nitrogen in the marine environment. Academic Press, pp 1-37

Schmid, A (1981) A thioredoxin activated glutamine synthetase in *Chlorella*. Z Naturforsch **36**: 396-399

Singh RP, Srivastava HS (1986) Increase in glutamate synthase (NADH) in maize seedlings in response to nitrate and ammonium nitrogen. Physiol Plant **66**: 413-416

Snell FD, Snell CT (1949) In "Colorimetric methods of analysis". Van Nostrand, New York, Vol II, pp 804-805

Song B, Ward BB (2007) Molecular cloning and characterization of high-affinity nitrate transporters in marine phytoplankton. J Phycol **43**: 542-552

Stolte W, Riegman R 1995 Effect of a phytoplankton cell size on transient-state nitrate and ammonium uptake kinetics. Microbiology **141**: 1221-1229

Tischner R, Hüttermann A (1980) Regulation of glutamine synthetase by light and during nitrogen deficiency in synchronous *Chlorella sorokiniana* Plant Physiol **66**: 805-808

Tischner R, Schmidt A (1982) A thioredoxin-mediated activation of glutamine synthetase and glutamate synthase in synchronous *Chlorella sorokiniana* Plant Physiol **70**: 113-116

Tortell PD (2000) Evolutionary and ecological perspectives on carbon acquisition in phytoplankton. Limnol Oceanogr **45**: 744-750

Trimborn S, Langer G, Rost B (2007) Effect of varying calcium concentrations and light intensities on calcification and photosynthesis in *Emiliania huxleyi*. Limnol Oceanogr **52**: 2285-2293

Tsuji Y, Suzuki I, Shiraiwa Y (2009) Photosynthetic carbon assimilation in the coccolithophorid *Emiliania huxleyi* (Haptophyta): Evidence for the predominant operation of the C_3 cycle and the contribution of β-carboxylases to the active anaplerotic reaction. Plant Cell Physiol **50**: 318-329

Turpin DH (1991) Effects of inorganic N availability on algal photosynthesis and carbon metabolism. J Phycol **27**: 14-20

Vanlerberghe G, Huppe HC, Vlossak KDM, Turpin DH (1992) Activation of respiration to support dark NO_3^- and NH_4^+ assimilation in the green alga *Selenastrum minutum*. Plant Physiol **99**: 495-500

Weger HG, Turpin DH (1989) Mitochondrial respiration can support NO_3^- and NO_2^- reduction during photosynthesis. Interactions between photosynthesis, respiration, and N assimilation in the N-limited green alga *Selenastrum minutum*. Plant Physiol **89**: 409-415

Weiner H, Kaiser WM (1999) 14-3-3 proteins control proteolysis of nitrate reductase in spinach leaves. FEBS **455**: 75-78

Williams PJI, Robertson JE (1991) Overall planktonic oxygen and carbon dioxide rnetabolisrns: the problem of reconciling observations and calculations of photosynthetic quotients. J Plankton Res **13**: 153-169

Winter A, Jordan RW, Roth PH 1994 Biogeography of living coccolithophores in ocean waters. In A Winter, Siesser WG, (eds), Coccolithophores. Cambridge Univ. Press, pp 161-177

Wolf-Gladrow DA, Riebesell U, Burkhardt S, Bijma J (1999) Direct effects of CO2 concentration on growth and isotopic composition of marine plankton, Tellus **51** (2): 461–476

Wray JL, Filner P (1970) Structural and functional relationships of enzyme activities induced by nitrate in barley. Biochem J **119**: 715-725

Young EB, Beardall J (2005) Modulation of photosynthesis and inorganic carbon acquisition in a marine microalga by nitrogen, iron, and light availability. Can J Bot **83**: 917-928

6. Acknowledgements

Ich möchte vor allem Jesus Christus für Alles danken.

Vielen dank an Scarlett Trimborn und Ellen Lichte für ihre Hilfe in der Laborarbeit während dieser Doktorarbeit.

Ich möchte Silke Thoms, Björn Rost, Gerald Langer, Klaus-Uwe Richter, Angela Köhler, Dieter Wolf-Gladrow, Allessandra Norici, Mario Giordano, Laurenz Thomsen, Sven Kranz, Sebastian Rokitta, Erika Allhusen, Matthias Köck und die Mitglieder der Gruppen der Biogeosciences und Zellbiologie/Toxikologie am AWI herzlich danken.

Ich möchte auch noch meiner Familie und meinen Freunden danken.

Own contributions

The PhD thesis with the title was conducted within three years from the 1st of February 2007 till the 31th of January 2010. In the first year I did several test-studies in order to identify the appropriate growth conditions for the phytoplankton species *Emiliania huxleyi* as well as the substrate concentrations needed for the kinetic measurements of enzyme and uptake kinetics. The actual experiment was run throughout the whole second year. During this period I took the samples and I conducted all the measurements stated in this thesis. The third year was dedicated into data processing and writing the manuscript for publishing, which has been submitted in the journal Plant Physiology.

I measured the concentrations of dissolved inorganic carbon and alkalinity in the alkalinity labour of the Biogeosciences group in the Alfred-Wegener-Institute. I took and prepared the samples for the elemental composition of *E. huxleyi* and they were measured in the Alfred-Wegener-Institute by the chemical engineer responsible for the mass spectrometer Mr. Klaus-Uwe Richter. I measured the protein amounts of algae samples with the Bradford method in the Tecan labour of the Cell biology and Toxicology group in the Alfred-Wegener-Institute. I prepared the samples for the determination of the macromolecular pools and they were sent to Italy to be measured with Fourier Transform Infrared Spectroscopy by Dr. Alessandra Norici from the University of Ancona. I prepared the samples for the assessment of coccolith morphology and Dr. Gerald Langer made the pictures with a scanning electron

microscope. I conducted the measurements for the nitrate assimilating enzymes in the Alfred-Wegener-Institute under the guidance of Prof. Dr. Angela Koehler. These measurements were done in the Tecan labour of the Cell biology and Toxicology group. Prof. Dr. Mario Giordano from the University of Ancona provided some standard protocols for enzyme measurements and helped in discussing the results of the experiment. The purification of the glutamine synthetase isoforms was conducted by high performance liquid chromatography with the help of Mrs. Ellen Lichte from the Ecological Chemistry group in the Alfred-Wegener-Institute. I made the measurements of photosynthesis, respiration and inorganic carbon acquisition in the Alfred-Wegener-Institute under the guidance of Dr. Scarlett Trimborn and Dr. Bjoern Rost. These measurements were done in the membrane inlet mass spectrometer labour of the Biogeosciences group. Dr. Silke Thoms is the project leader, and she contributed significant in this work with her help in discussing the data and writing the manuscript.

Athanasios Kaffes Bremerhaven, 19th of January 2010